
WAVE PROPAGATION THROUGH PERIODIC ARRAYS OF FREELY FLOATING RECTANGULAR FLOES

A PREPRINT

Lloyd Dafydd & Richard Porter

March 17, 2026

ABSTRACT

The two-dimensional propagation of small-amplitude waves through an infinite periodic array of freely-floating rectangular floes is considered under the assumptions of inviscid linearised wave theory. Fluid gaps between adjacent floes allow a complex interaction of the fluid with heave, surge and pitch motions. In particular, the presence of fluid resonance in the vertical channels between floes has a significant influence on wave propagation around certain critical frequencies. Bloch-Floquet theory is used and encodes the wavenumber for propagating waves into periodic boundary conditions. Solutions of the resulting boundary-value problem posed in a fundamental cell are formulated in terms of integral equations in which the three rigid body modes of the problem are treated individually. The dispersion relationship between frequency and wavenumber is expressed in terms of the vanishing of a 3×3 determinant which encodes the hydrodynamic coupling between the modes. Accurate numerical solutions are determined using Galerkin's method to approximate solutions to the integral equations. A particular focus of the paper is determining simple explicit approximations for the dispersion relation by assuming the gap between adjacent floes is small compared to the submerged draft of the floe. Approximations are shown to compare well to numerical results for a large range of gap sizes and some surprising results emerge for low-frequency wave propagation. This is particularly relevant to the application area that motivates this study: the modelling of wave propagation through broken ice.

1 Introduction

In two recent papers by the authors Dafydd and Porter (2024, 2026), the two-dimensional propagation of waves through broken floating ice of randomly-varying thickness was studied. Their primary purpose was to consider whether randomness could provide an explanation for the observed frequency-dependent attenuation of ocean-ice coupled waves within the Marginal Ice Zones: regions of fragmented sea ice on the boundary of the open ocean and the shore-fast sea ice. For a further description see the reviews of Squire (2018), Meylan et al. (2018) and the many papers cited therein. In the models of Dafydd and Porter (2024, 2026) it is assumed that fragmented ice completely covers the surface of the ocean with no fluid gaps between neighbouring floes which are constrained to move vertically (in *heave*, in the language of ship hydrodynamics). This choice of model was made for simplicity and extends the widely-used mass-loading model (see Weitz and Keller (1950), Mosig et al. (2017) and others) to ice of slowly-varying thickness. Explicit theoretical predictions of the attenuation due to wave scattering through random environments (often referred in other physical contexts as localisation) made by Dafydd and Porter (2024, 2026) were confirmed by numerical simulations. Thus the dependence of attenuation with frequency, f , was shown to be proportional to f^2 in shallow water and to f^8 in deep water (both results applying for low frequencies). However these results are not aligned with field measurements (see, for example, Meylan et al. (2014), Doble et al. (2015), Rogers et al. (2016), Hošeková et al. (2020)) which suggest the functional attenuation dependence on frequency of between f^2 and f^4 . On the other hand some features of the theoretical results of Dafydd and Porter (2024, 2026) compared more favourably with the data. Specifically, this included a quadratic relation between ice thickness and attenuation and the prediction of a high-frequency 'rollover effect' (see Li et al. (2018)), a persistent feature of datasets in many field measurements (see Wadhams et al. (1988), Doble et al. (2015) for example) although recently theorised by Thomson et al. (2021) to be a statistical effect produced by noisy data.

The purpose of the present paper is to consider how the introduction of gaps between adjacent floes in the broken ice cover might affect wave propagation. Specifically, this paper aims to answer the question: is the zero-gap heave-constrained (or mass loading) model used in Dafydd and Porter (2024, 2026) a reasonable approximation to the more physically realistic scenario of a broken ice cover which includes small gaps? A positive answer to the question would confirm the validity of the earlier, simple, model. A negative answer allows for the possibility that the theoretical prediction of attenuation may be altered by the introduction of gaps between floes.

Adopting the notion of a slow spatial variation in the floe characteristics, a key assumption of the models used by Dafydd and Porter (2024, 2026), allows us to consider a simpler problem in which waves propagate locally as though they were within an infinite periodic array of identical floes with equally-spaced gaps between neighbouring floes (see the arguments of Allaire (1992) for example). This argument allows us to simplify the problem, using Bloch-Floquet theory, to a single floe in a single fundamental cell with the extension to other periods in the array made through the introduction of periodic boundary conditions. The Bloch-Floquet wavenumber which is encoded into the lateral cell boundary conditions plays the role of the local wavenumber of propagating waves and its dependence upon frequency in this unforced (i.e. spectral) problem gives rise to a dispersion relation. Determining this dispersion relation and its relationship to the size and shape of the floes and the gaps between them is our main goal which we approach both theoretically and numerically.

Within the fundamental cell the floating rectangular floe is allowed to move freely in heave, surge and pitch motions. Each rigid-body mode of motion is coupled to the other two modes via the fluid and is manifested by (9 in total) fundamental hydrodynamic forces. The coupling is encoded within the dynamic equations (as describe ship motions; see Newman (1977) or Mei et al. (2005)) of heave, surge and pitch and thus the dispersion relation is expressed as the vanishing determinant of a 3×3 matrix. We establish the governing system described above in Section 2 of the paper.

The generality of the current work appears to make it somewhat distinct from other problems in the literature. In terms of considering two-dimensional wave propagation through floating structures, Chou (1998) considered waves through periodic arrays of flexible floating ice sheets, whilst there are more examples of waves interacting with two-dimensional periodic arrays of fixed structures (for example, Linton (2011), Huang and Porter (2023)) and periodic beds (for example Davies and Heathershaw (1984)). The majority of the mathematical models that approximate the propagation of waves through regions of floating ice treat the ice as flexible but with zero draft; many examples are listed in the review of Squire (2025), but see Pitt and Bennetts (2026) for a recent example. This description allows heave and pitch motions to be captured (in addition to any flexural waves through the ice/fluid coupling; only relevant for sufficiently large floes) but surge motions are not. Notable exceptions include the work of Meylan et al. (2015), Shen and Ackley (1991). Examples of work in the class of spectral problems which involve periodic arrays of freely-floating rigid bodies include Dias and Videman (2014) and Carter and McIver (2013).

The assumption of rectangular floes allow the solution to each of the three independent components of the problem (forced heave, surge and pitch) to be expressed in terms of integral equations which arise from matching separation solutions at the common interface between two rectangular fluid regions. This is a non-trivial exercise especially in the case of forced pitch where both the sides and the base of the floe are in prescribed motion. Because of this we outline the solution procedure is detailed in Section 3 of the paper for the case of problem in which the floe moves in heave. Section 3 also includes the application of the numerical approximation method and asymptotic methods for small gaps for the case of heave-constrained motion. To avoid swamping the paper with excessive complicated algebra, the detailed solution for the remaining problems of surge and pitch are relegated to the supplementary paper and include the associated numerical methods and asymptotic approximations. In Section 4 we focus attention on the explicit expressions required to describe the dispersion for wave propagation in the presence of small gaps between neighbouring ice floes. These asymptotic solutions are related to the full numerical solutions across a suite of results showing the different isolated and coupled effects of heave, surge and pitch. In Section 5 we present and discuss results for the fully unconstrained problem and we present our conclusions in Section 6.

2 Definition of the problem

Without loss of generality we arrange the coordinate system such that the x axis is aligned with the rest position of the fluid surface and the z axis is directed vertically upwards in line with the reference position of the right side of a floe in the periodic array (see Fig. 1). The width of the period is defined by L and $\ell < L$ is the width of the fluid between opposing parallel sides of adjacent floes. Within the fundamental cell, defined as $0 < x < L$, the reference position describing floe/fluid boundaries include: the floe base along $z = -\hat{\rho}d$, $\ell < x < L$; its left side $x = \ell$, $-\hat{\rho}d < z < 0$ and the right-hand side of floe in the neighbouring period, floe is $x = 0$, $-\hat{\rho}d < z < 0$. Here $\hat{\rho} = \rho_f/\rho < 1$ represents the ratio of floe and fluid densities. The off-centre choice of geometry is made to simplify the fluid domain in a fundamental cell so that it is comprised of the union of two rectangular domains labelled V^\pm in Fig. 1.

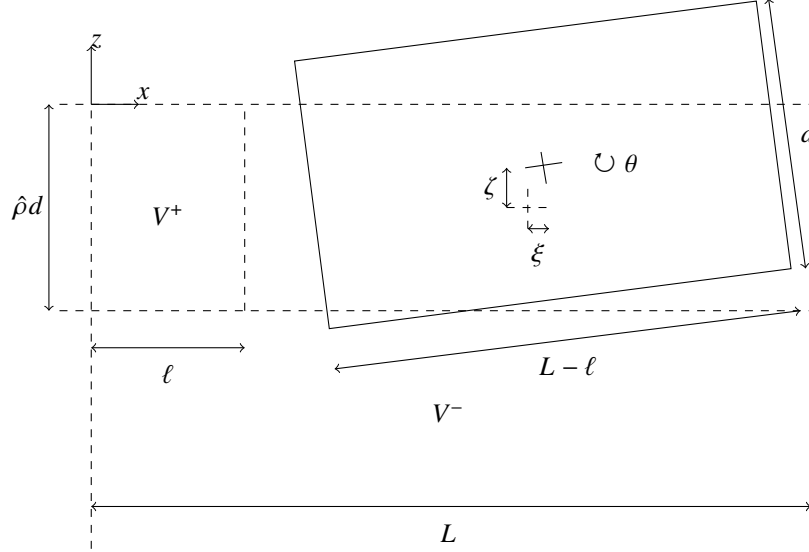


Figure 1: Definition of the coordinate system and variables used

Inviscid potential theory is used to describe the assumed small-amplitude irrotational motion of an incompressible fluid in which the fluid velocity equals $\Re\{\nabla\phi e^{-i\omega t}\}$ having assumed a harmonic time dependence of angular frequency ω . The floe in $0 < x < L$ moves in response to the fluid with given oscillatory heave and surge displacements $\Re\{\zeta e^{-i\omega t}\}$ and $\Re\{\xi e^{-i\omega t}\}$ and a (clockwise) pitch angle $\Re\{\theta e^{-i\omega t}\}$. These oscillations are made about the reference position of the floe stated previously.

In the fluid

$$\nabla^2 \phi = 0 \quad (2.1)$$

with $|\nabla\phi| \rightarrow 0$ as $z \rightarrow -\infty$ (it is assumed the fluid is infinitely deep). The combined linearised kinematic and dynamic free surface conditions can be expressed as

$$\phi_z - K\phi = 0, \quad \text{on } z = 0, \quad 0 < x < \ell \quad (2.2)$$

where $K = \omega^2/g$. The linearised kinematic condition on the base of the floe is given by

$$\phi_z = -i\omega(\zeta - (x - x^c)\theta), \quad \text{on } z = -\hat{\rho}d, \quad \ell < x < L \quad (2.3)$$

where $x^c = \frac{1}{2}(\ell + L)$ denotes the centre of the floe. We also have Bloch-Floquet boundary conditions

$$\phi(L, z) = e^{ikL}\phi(0, z), \quad \phi_x(L, z) = e^{ikL}\phi_x(0, z) \quad (2.4)$$

for $z < -\hat{\rho}d$ where kL is the dimensionless Bloch wavenumber implying that the solution may be extended beyond $0 < x < L$ using $\phi(x + mL, z) = e^{imkL}\phi(x, z)$ for $m \in \mathbb{Z}$. On the sidewalls of the floe, the linearised kinematic conditions are

$$\phi_x(\ell, z) = -i\omega(\xi + (z - z^c)\theta), \quad \text{on } -\hat{\rho}d < z < 0 \quad (2.5)$$

and

$$\phi_x(0, z) = -i\omega e^{ikL}(\xi + (z - z^c)\theta), \quad \text{on } -\hat{\rho}d < z < 0 \quad (2.6)$$

where $z^c = (\frac{1}{2} - \hat{\rho})d$ is the vertical coordinate of the rest position of the centre of the floe, determined by Archimedes' law. The dynamic equations, measured in relation to the centre of mass, (x^c, z^c) , for heave, surge and pitch are (see Newman (1977))

$$-\omega^2 \rho_f \zeta (L - \ell) d = -\rho g (L - \ell) \zeta + i\omega \rho \int_{\ell}^L \phi(x, -\hat{\rho}d) dx \quad (2.7)$$

and

$$-\omega^2 \rho_f \xi (L - \ell) d = i\omega \rho \int_{-\hat{\rho}d}^0 \phi(\ell, z) - e^{ikL} \phi(0, z) dz \quad (2.8)$$

and

$$\begin{aligned}
-\omega^2 \frac{1}{12} \rho_f (L - \ell) d ((L - \ell)^2 + d^2) \theta &= -\frac{1}{12} \rho g (L - \ell)^3 \theta + \frac{1}{2} \rho_f g d^2 (1 - \hat{\rho}) (L - \ell) \theta \\
&\quad - i\omega \rho \int_{\ell}^L (x - x^c) \phi(x, -\hat{\rho}d) dx + i\omega \rho \int_{-\hat{\rho}d}^0 (z - z^c) \left(\phi(\ell, z) - e^{ikL} \phi(0, z) \right) dz \quad (2.9)
\end{aligned}$$

where periodicity has been used to relate forces and moments along $x = L$ to the boundary along $x = 0$ lying within the fundamental period.

The first two terms on the right-hand side of (2.9) are contributions to hydrostatic restoring forces from the base and side-walls of the floe respectively. These first-order terms arise, like the first term in (2.7), from integrating the hydrostatic component of the pressure over the instantaneous wetted surface of the floe in motion. All first-order hydrodynamic contributions to the pressure are integrated over the mean wetted surface.

The problem set out above is homogeneous and requires us to establish the relationship between the wavenumber, k , and the frequency parameter $K = \omega^2/g$. To do this we separate the contributions from the three motions by writing

$$\phi(x, z) = -i\omega \left(\zeta \phi^{(h)}(x, z) + \xi \phi^{(s)}(x, z) + (L - \ell) \theta \phi^{(p)}(x, z) \right) \quad (2.10)$$

where $\phi^{(h,s,p)}$ are required to satisfy (2.1), (2.2) and (2.4) along with the additional boundary conditions on the floes consisting of

$$\phi_z^{(h)}(x, -\hat{\rho}d) = 1, \quad \phi_z^{(s)}(x, -\hat{\rho}d) = 0, \quad \phi_z^{(p)}(x, -\hat{\rho}d) = -(x - x^c)/(L - \ell) \quad (2.11)$$

for $\ell < x < L$ and

$$\phi_x^{(h)}(\ell, z) = 0, \quad \phi_x^{(s)}(\ell, z) = 1, \quad \phi_x^{(p)}(\ell, z) = (z - z^c)/(L - \ell) \quad (2.12)$$

with $\phi_x^{(h,s,p)}(0, z) = e^{-ikL} \phi_x^{(h,s,p)}(\ell, z)$ for $-\hat{\rho}d < z < 0$.

Quantities of interest that will be sought from the solution to the problems for $\phi^{(h,s,p)}$ are components proportional to the dynamic heave and surge forces and pitch moments on the base and the sidewalls due to fluid motion. We define the normalised dynamic force in mode $b \in \{h, s, p\}$ due to forced motion in mode $a \in \{h, s, p\}$ by

$$\begin{aligned}
F^{(a,b)} &= \frac{1}{d(L - \ell)} \int_{\ell}^L \phi^{(a)}(x, -\hat{\rho}d) \overline{\phi_z^{(b)}(x, -\hat{\rho}d)} dx \\
&\quad + \frac{1}{d(L - \ell)} \int_{-\hat{\rho}d}^0 \phi^{(a)}(\ell, z) \overline{\phi_x^{(b)}(\ell, z)} - \phi^{(a)}(0, z) \overline{\phi_x^{(b)}(0, z)} dz. \quad (2.13)
\end{aligned}$$

For example, the heave induced force due to forced heave, surge or pitch motions is

$$F^{(a,h)} = \frac{1}{d(L - \ell)} \int_{\ell}^L \phi^{(a)}(x, -\hat{\rho}d) dx \quad (2.14)$$

where $a \in \{h, s, p\}$.

Thus, the strategy is to solve each hydrodynamic problem for $\phi^{(h,s,p)}$ in order to compute these quantities and then, using (2.10) in (2.7)–(2.9) with the definition (2.13), we have the system of equations

$$\begin{pmatrix}
1 - Kd(\hat{\rho} + F^{(h,h)}) & -KdF^{(s,h)} & -KdF^{(p,h)} \\
-KdF^{(h,s)} & -Kd(\hat{\rho} + F^{(s,s)}) & -KdF^{(p,s)} \\
-KdF^{(h,p)} & -KdF^{(s,p)} & \frac{1}{12} - \frac{1}{2}\hat{\rho}(1 - \hat{\rho})\hat{d}^2 - \frac{1}{12}K\hat{\rho}d(1 + \hat{d}^2) - KdF^{(p,p)}
\end{pmatrix}
\begin{pmatrix}
\zeta \\
\xi \\
(L - \ell)\theta
\end{pmatrix} = 0 \quad (2.15)$$

where $\hat{d} = d/(L - \ell)$ is the aspect ratio of the floe. Eigensolutions of (2.15) determine k as a function of K and the corresponding floe motions. The matrix in (2.15) is often presented as the sum of three matrices representing the solid inertia, added fluid inertia (both proportional to ω^2) and hydrostatic restoring forces. In this respect the absence of the usual exciting forces and radiation damping components is expected since the fluid motion is unforced and energy is confined within the finite domain. Note that we require $\hat{d} < 1/\sqrt{6\hat{\rho}(1 - \hat{\rho})}$ for static stability of the rectangular floe.

If we have two functions φ and χ that are harmonic in the domain V , Green's identity states that

$$\int_S \frac{\partial \varphi}{\partial n} \chi - \frac{\partial \chi}{\partial n} \varphi ds = 0 \quad (2.16)$$

where s measures the arclength on S , which is a closed surface around V , and the normal derivative is directed outwards from V . Now if, for example, we let $\varphi = \phi^{(a)}$ and $\chi = \phi^{(b)}$ in the domain occupied by the fluid and apply (2.2), (2.4), (2.11) and (2.12) we get the reciprocity relation

$$F^{(a,b)} = \overline{F^{(b,a)}}. \quad (2.17)$$

Clearly, this implies for all $a \in h, s, p$ we have that $F^{(a,a)}$ is real and the matrix in (2.15) is Hermitian (assuming $K \in \mathbb{R}$) and therefore has real eigenvalues. It is the vanishing of one of those eigenvalues that determines solutions. The corresponding eigenvectors provide information about the motion itself.

3 Solution in heave

A general expression for $\phi^{(h)}(x, z)$ in the fluid region $V^+ := \{0 < x < \ell, -\hat{\rho}d < z < 0\}$ (see Fig. 1) satisfying both (2.1) and (2.11) can be written in terms of the series

$$\phi^{(h)}(x, z) = \sum_{m=0}^{\infty} a_m Z_m(z) \cos \alpha_m x \quad (3.1)$$

where $\alpha_m = m\pi/\ell$ and

$$Z_0(z) = 1 + Kz, \quad Z_m(z) = \cosh \alpha_m z + (K/\alpha_m) \sinh \alpha_m z \quad (3.2)$$

are chosen to satisfy (2.2). Using the orthogonality result

$$\frac{1}{\ell} \int_0^{\ell} \cos \alpha_m x \cos \alpha_n x \, dx = \begin{cases} 1, & m = n = 0, \\ \frac{1}{2}, & m = n \neq 0, \\ 0, & \text{otherwise} \end{cases} \quad (3.3)$$

we can express the unknown coefficients a_m in (3.1) as

$$a_0 = \frac{1}{K\ell} \int_0^{\ell} W^{(h)}(x) \, dx \quad (3.4)$$

and

$$(K \cosh(\alpha_m \hat{\rho}d) - \alpha_m \sinh(\alpha_m \hat{\rho}d)) a_m = \frac{2}{\ell} \int_0^{\ell} W^{(h)}(x) \cos \alpha_m x \, dx \quad (3.5)$$

for $m \geq 1$ in terms of $W^{(h)}(x) \equiv \phi_z^{(h)}(x, -\hat{\rho}d)$, defined over $0 < x < \ell$ to be the vertical component of the fluid velocity across the interface between the two rectangular fluid sub-domains V^+ and $V^- := \{z < -\hat{\rho}d, 0 < x < L\}$.

In V^- , we require solutions to satisfy (2.1), (2.4) and (2.12) and find a general solution can be written

$$\phi^{(h)}(x, z) = \varphi^{(h)}(x, z) + \sum_{m=-\infty}^{\infty} b_m e^{i\beta_m x} e^{\beta_m(z+\hat{\rho}d)} \quad (3.6)$$

where $\beta_m = k + 2\pi m/L$. Here, we define $\varphi^{(h)}(x, z)$ to be a harmonic function in the region $z < -\hat{\rho}d, 0 < x < L$ satisfying the periodicity conditions (2.4) and decaying as $z \rightarrow -\infty$ which is used to absorb the inhomogeneous condition (2.11) by defining

$$\varphi_z^{(h)}(x, -\hat{\rho}d) = \begin{cases} 1, & \ell < x < L \\ 0, & 0 < x < \ell \end{cases} \quad (3.7)$$

leaving the second term in (3.6) to satisfy a homogeneous Neumann condition on $z = -\hat{\rho}d, \ell < x < L$. From this prescription for $\varphi^{(h)}(x, z)$ is straightforward to determine that

$$\varphi^{(h)}(x, z) = \ell \sum_{m=-\infty}^{\infty} \frac{g_m^{(h)} e^{i\beta_m x}}{\beta_m L} e^{\beta_m(z+\hat{\rho}d)} \quad (3.8)$$

where

$$g_m^{(h)} = \frac{1}{\ell} \int_{\ell}^L e^{-i\beta_m x} \, dx = \frac{1}{i\beta_m \ell} \left(e^{-i\beta_m \ell} - e^{-i\beta_m L} \right). \quad (3.9)$$

In deriving the result above we have used the orthogonality relation

$$\frac{1}{L} \int_0^L e^{i\beta_m x} e^{-i\beta_n x} \, dx = \begin{cases} 1, & m = n \\ 0, & \text{otherwise.} \end{cases} \quad (3.10)$$

Returning to (3.6), it is clear we can now also express the coefficients in the series in terms of the function $W^{(h)}(x)$ so that

$$b_m = \frac{1}{\beta_m L} \int_0^{\ell} W^{(h)}(x) e^{-i\beta_m x} \, dx \quad (3.11)$$

for all m .

The only remaining condition of the problem is to ensure the continuity of $\phi^{(h)}$ across the interface $z = -\hat{\rho}d, 0 < x < \ell$. Thus, from (3.1) and (3.6) and definitions for a_m and b_m we arrive at the integral equation

$$(\mathcal{T}W^{(h)})(x) = \frac{1}{\ell} \int_0^\ell W^{(h)}(x')T(x, x') dx' = G^{(h)}(x), \quad 0 < x < \ell \quad (3.12)$$

for the function $W^{(h)}(x)$ where

$$T(x, x') = \frac{K\hat{\rho}d - 1}{K\ell} + 2 \sum_{m=1}^{\infty} \frac{(K \tanh(\alpha_m \hat{\rho}d) - \alpha_m) \cos \alpha_m x \cos \alpha_m x'}{\alpha_m \ell (K - \alpha_m \tanh(\alpha_m \hat{\rho}d))} + \sum_{m=-\infty}^{\infty} \frac{e^{i\beta_m(x-x')}}{\beta_m L} \quad (3.13)$$

defines the kernel of the integral operator \mathcal{T} and where

$$G^{(h)}(x) = -(1/\ell)\varphi^{(h)}(x, -\hat{\rho}d) = - \sum_{m=-\infty}^{\infty} \frac{g_m^{(h)} e^{i\beta_m x}}{\beta_m L} \quad (3.14)$$

represents the forcing term. We note that $T(x, x') = \overline{T(x', x)}$ is Hermitian and hence \mathcal{T} is self-adjoint. The solution of (3.12) can be used to determine ϕ everywhere in the fluid. However, our primary goal is to compute $F^{(h,h)}$ as defined by (2.14) and we consider this next.

Using Green's identity with $\phi^{(h)}(x, z)$ and $\overline{\varphi^{(h)}}(x, z)$, in the domain V^- with boundary ∂V^- , gives us

$$0 = \int_{\partial V^-} \frac{\partial \phi^{(h)}}{\partial n} \overline{\varphi^{(h)}} - \frac{\partial \overline{\varphi^{(h)}}}{\partial n} \phi^{(h)} ds \quad (3.15)$$

$$= \int_0^\ell \left(\frac{\partial \phi^{(h)}}{\partial z} \overline{\varphi^{(h)}} - \frac{\partial \overline{\varphi^{(h)}}}{\partial z} \phi^{(h)} \right)_{z=-\hat{\rho}d} dx + \int_\ell^L \left(\frac{\partial \phi^{(h)}}{\partial z} \overline{\varphi^{(h)}} - \frac{\partial \overline{\varphi^{(h)}}}{\partial z} \phi^{(h)} \right)_{z=-\hat{\rho}d} dx \quad (3.16)$$

$$= \int_0^\ell W^h(x) \overline{\varphi^{(h)}}(x, -\hat{\rho}d) dx + \int_\ell^L \overline{\varphi^{(h)}}(x, -\hat{\rho}d) - \phi^{(h)}(x, -\hat{\rho}d) dx \quad (3.17)$$

using conditions satisfied by $\phi^{(h)}(x, z)$ and $\varphi^{(h)}(x, z)$ and so it follows that

$$\int_\ell^L \phi^{(h)}(x, -\hat{\rho}d) dx = \int_0^\ell W^{(h)}(x) \overline{\varphi^{(h)}}(x, -\hat{\rho}d) dx + \int_\ell^L \overline{\varphi^{(h)}}(x, -\hat{\rho}d) dx. \quad (3.18)$$

Using the definition (2.13), the relation (3.14) and (3.18) results in

$$F^{(h,h)} = -\frac{\ell^2}{(L-\ell)d} A^{(h,h)} + C^{(h,h)} \quad (3.19)$$

where, for convenience, here we have defined

$$A^{(h,h)} = \frac{1}{\ell} \int_0^\ell W^{(h)}(x) \overline{G^{(h)}}(x) dx \quad (3.20)$$

and

$$C^{(h,h)} = \frac{\ell^2}{(L-\ell)d} \sum_{m=-\infty}^{\infty} \frac{|g_m^{(h)}|^2}{\beta_m L} = \frac{(L-\ell)}{2d} \cot(kL/2) \quad (3.21)$$

where the cot term arises from evaluating the infinite sum using contour integration (see equation (S.A.13) in Appendix A of the supplementary material). The manipulations above have allowed us to express $F^{(h,h)}$, as required by (2.15), directly in terms of the solution $W^{(h)}(x)$ of the integral equation (3.12). This formulation, along with the explicit evaluation of the series defining $C^{(h,h)}$ in (3.21), is crucial for approximating solutions as we shall show in Section 3.2.

3.1 Numerical solution

In order to approximate (3.19) to arbitrary precision we use Galerkin's method which involves approximating the solution of the integral equation (3.12) as an expansion

$$W^{(h)}(x) \approx \sum_{n=0}^N A_n u_n(x) \quad (3.22)$$

in terms of a set of basis functions $u_n(x)$ (to be defined in a moment) and unknown coefficients A_n ; N is a truncation parameter. After substituting (3.22) into (3.12), multiplying by $\overline{u_m(x)}$ and integrating over $0 < x < \ell$, a process which characterises Galerkin's method, one obtains the linear system of equations

$$\sum_{n=0}^N A_n T_{mn} = E_m^{(h)} \quad (3.23)$$

defining A_n where

$$T_{mn} = \langle \mathcal{T} u_n, u_m \rangle \quad (3.24)$$

and

$$E_m^{(h)} = \langle G^{(h)}, u_m \rangle \quad (3.25)$$

are prescribed, the notation $\langle u, v \rangle$ being employed here as shorthand for the inner product $\ell^{-1} \int_0^\ell u(x) \overline{v(x)} dx$.

Using (3.22) in (3.20) gives

$$A^{(h,h)} \approx \sum_{n=0}^N A_n \overline{E_n^{(h)}}. \quad (3.26)$$

If we define

$$\mathcal{I}_{mn} = \langle \cos \alpha_n x, u_m \rangle \quad \text{and} \quad \mathcal{J}_{mn} = \langle e^{i\beta_n x}, u_m \rangle \quad (3.27)$$

it follows from (3.24) that

$$T_{mn} = \frac{K\hat{\rho}d - 1}{K\ell} \mathcal{I}_{m0} \overline{\mathcal{I}_{n0}} + 2 \sum_{r=1}^{\infty} \frac{K \tanh(\alpha_r \hat{\rho}d) - \alpha_r}{\alpha_r \ell (K - \alpha_r \tanh(\alpha_r \hat{\rho}d))} \mathcal{I}_{mr} \overline{\mathcal{I}_{nr}} + \sum_{r=-\infty}^{\infty} \frac{1}{\beta_r L} \mathcal{J}_{mr} \overline{\mathcal{J}_{nr}} \quad (3.28)$$

and, from (3.14), that

$$E_m^{(h)} = - \sum_{r=-\infty}^{\infty} \frac{g_r^{(h)}}{\beta_r L} \mathcal{J}_{mr}. \quad (3.29)$$

With the knowledge that $W^{(h)}(x)$ is proportional to the vertical velocity of the flow across the opening $z = -\hat{\rho}d$, $0 < x < \ell$, $W^{(h)}(x) \sim C_0 x^{-1/3}$ as $x \rightarrow 0^+$ and $W^{(h)}(x) \sim C_\ell (\ell - x)^{-1/3}$ as $x \rightarrow \ell^-$ (C_0, C_ℓ constants) corresponding to the local flow of an ideal fluid around a right-angled corner. To preserve a simple form of T_{mn} , we choose (see Evans and Fernyhough (1995), for example)

$$u_m(x) = \frac{i^m (m!) \Gamma(\frac{1}{6}) \ell^{2/3}}{\sqrt{2\pi} \Gamma(m + \frac{1}{3}) x^{1/3} (\ell - x)^{1/3}} C_m^{1/6} \left(\frac{2x - \ell}{\ell} \right) \quad (3.30)$$

where C_n^ν represents the orthogonal ultraspherical Gegenbauer polynomials. With the help of Evans and Fernyhough (1995) the following results can be derived:

$$\mathcal{I}_{m0} = \frac{6}{2^{1/6} \Gamma(\frac{1}{6})} \delta_{m0}; \quad (3.31)$$

$$\mathcal{I}_{mn} = (-i)^m \cos\left((m+n) \frac{\pi}{2}\right) \frac{J_{m+1/6}(n\pi/2)}{(n\pi/2)^{1/6}} \quad (3.32)$$

for $n \geq 1$; and

$$\mathcal{J}_{mn} = (-1)^m e^{i\beta_n \ell/2} J_{m+1/6}(\beta_n \ell/2) / (\beta_n \ell/2)^{1/6}. \quad (3.33)$$

3.2 Heave-constrained motion and small gaps

If we assume the floe motion is constrained to move in heave only then from (2.15) the condition for propagating waves is reduced to

$$Kd(\hat{\rho} + F^{(h,h)}) = 1. \quad (3.34)$$

Let us consider $\epsilon = \ell/d \ll 1$. Further, it will be assumed that $|K\hat{\rho}d - 1| \gg \epsilon$; this avoids fluid resonance in narrow fluid channels which is associated with the condition $K\hat{\rho}d = 1$. It follows from (3.13), after using (S.B.3), that

$$T(x, x') \approx \frac{1}{\epsilon} \tilde{T}(x, x'), \quad \text{where} \quad \tilde{T}(x, x') = \frac{K\hat{\rho}d - 1}{Kd} + \frac{1}{2} \epsilon \cot\left(\frac{kL}{2}\right) \quad (3.35)$$

and tildes are used henceforth to denote terms of $O(1)$ with respect to ϵ . The second term is included since it can also contribute at $O(1)$ in the wavenumber intervals $kL \lesssim O(\epsilon)$ and $2\pi - kL \lesssim O(\epsilon)$ where $\cot(kL/2) = O(1/\epsilon)$. This turns out to have a significant effect on some of the asymptotic results we encounter whose dispersion curves cross, or lie within, the small wavenumber intervals close to $kL = 0$ and $kL = 2\pi$. In other cases it has less of an effect. For example, the result (3.44) below does not change when the second term in (3.35) is removed.

We also find that, since $0 < x < \ell$,

$$G^{(h)}(x) \approx \frac{1}{\epsilon} \tilde{G}^{(h)}, \quad (3.36)$$

where, from (3.9), (3.14), we have

$$\tilde{G}^{(h)} = i \frac{L}{d} (1 - e^{-ikL}) \sum_{m=-\infty}^{\infty} \frac{1}{(\beta_m L)^2} = i \frac{L}{4d} (1 - e^{-ikL}) \operatorname{cosec}^2\left(\frac{kL}{2}\right) \quad (3.37)$$

after using Gradshteyn and Ryzhik (1981) §1.422(4).

It follows upon using (3.35) and (3.36) in (3.12) that

$$\frac{1}{\ell} \int_0^\ell W^{(h)}(x') dx' \approx \tilde{G}^{(h)} / \tilde{T} \quad (3.38)$$

and then, together with (3.19), that

$$F^{(h,h)} \approx C^{(h,h)} - \epsilon \frac{d}{L - \ell} |\tilde{G}^{(h)}|^2 / \tilde{T}. \quad (3.39)$$

Full simplification of the result above results in

$$F^{(h,h)} \approx F_0^{(h,h)} + \epsilon F_1^{(h,h)} \quad (3.40)$$

where

$$F_0^{(h,h)} = \frac{L}{2d} \cot(kL/2), \quad F_1^{(h,h)} = -\frac{1}{2} \cot(kL/2) - \frac{KL \operatorname{cosec}^2\left(\frac{kL}{2}\right)}{4(K\hat{\rho}d - 1) + 2\epsilon Kd \cot(kL/2)}. \quad (3.41)$$

Using this in (3.34) gives the approximate dispersion relation for heave-constrained motion with small gaps as

$$\frac{1 - K\hat{\rho}d}{Kd} \approx \frac{L \cot(kL/2)}{2d} - \epsilon \left(\frac{1}{2} \cot\left(\frac{kL}{2}\right) + \frac{KL \operatorname{cosec}^2\left(\frac{kL}{2}\right)}{4(K\hat{\rho}d - 1) + 2\epsilon Kd \cot(kL/2)} \right). \quad (3.42)$$

We can solve this for k in terms of K by letting $\cot(kL/2) \equiv X \approx X_0 + \epsilon X_1 + \dots$ in (3.42) and matching term-by-term to get

$$X_0 = \kappa \equiv \frac{2(1 - K\hat{\rho}d)}{KL}, \quad X_1 = -(d/L)/\kappa \quad (3.43)$$

and so

$$k \approx \frac{2}{L} \cot^{-1}\left(\kappa - \epsilon \frac{d}{LK}\right). \quad (3.44)$$

This result ensures that kL is 2π -periodic as required by the problem whereas further Taylor expansion of the inverse cot function destroys this property.

We note that when $\epsilon \rightarrow 0$, (3.44) reduces to

$$k \approx \frac{2}{L} \cot^{-1}\left(\frac{2(1 - K\hat{\rho}d)}{KL}\right) \quad (3.45)$$

which is therefore the exact dispersion relation for heave-constrained motion in the case that there are no fluid gaps. In the case the underlying wavelength is long compared to the width of the floes ($KL \ll 1$) (3.45) reduces further to

$$k \approx \frac{K}{(1 - K\hat{\rho}d)}, \quad (3.46)$$

now independent of L , and coincides with the mass loading model of Weitz and Keller (1950) and the dispersion relation used in Dafydd and Porter (2026) when d is taken to be a slowly-varying function of x .

3.3 Results for heave constrained motion

In Fig. 2 we provide a comparison between the full numerical results based on the methods described in Section 3.1 with the various asymptotic results derived in Section 3.2. We have chosen to focus on the case where $(L - \ell) = d$, and $\hat{\rho} = 0.9$ corresponding to a square ice block. The effect of the increasing the size of the fluid gap between adjacent ice blocks is considered by setting $\epsilon = \ell/d = 0.01, 0.02, 0.08, 0.12$. Each subplot shows: the full numerical solution of the dispersion relation; the leading-order approximation, as given by (3.45), which is independent of ϵ ; the explicit $O(\epsilon)$ approximation given by (3.44); and a solution which simply root-finds solutions to (3.42). The explicit $O(\epsilon)$ solution provides a very good fit to the full numerical results for all gap sizes considered and across all frequencies, including close to resonance ($K\hat{\rho}d = 1$), to the extent that the curves are near indistinguishable in Figure 2. Pure root-finding introduces discrepancies near $kL, 2\pi - kL \approx 0$ due to inconsistencies introduced when expanding to $O(\epsilon)$; it is important to note that these are not associated with the retention of the second term in (3.35). These issues will not arise in surge and pitch constrained results where asymptotic expansions will be limited to leading order, although these effects will reemerge when other modes are coupled to heave.

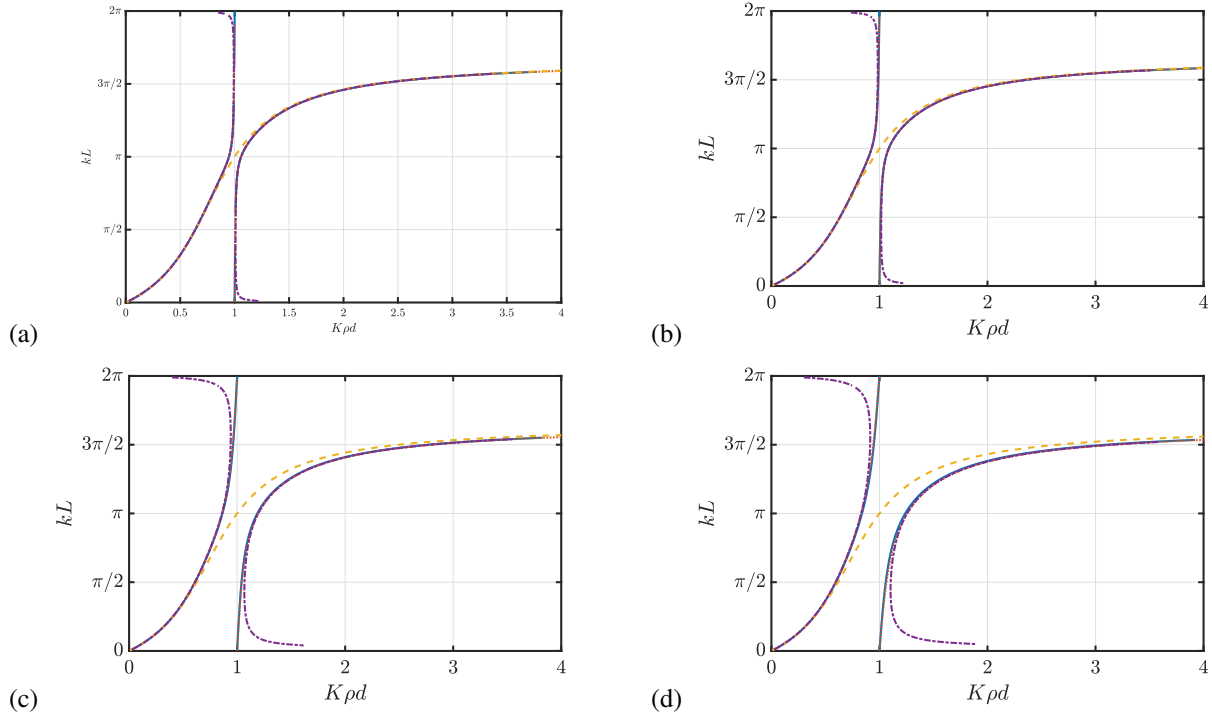


Figure 2: Dispersion curves (kL versus $K\hat{\rho}d$) for heave-constrained motions in the case $\hat{\rho} = 0.9$, $L/d = 1 + \epsilon$ (square ice floes). Exact results (blue solid curves), explicit $O(\epsilon)$ small-gap approximation (orange, dotted), leading order small-gap approximation (yellow, dashed) and small gap root-finding (purple, dot-dashed) for gap sizes: (a) $\epsilon = 0.01$, (b) $\epsilon = 0.02$, (c) $\epsilon = 0.08$, (d) $\epsilon = 0.12$.

4 Solutions in surge and pitch

We can continue with a similar analysis for the other two modes of motion, surge and pitch, and hence determine forces which are associated with these motions. Since the details are long and algebraically complicated, we have relegated them to a supplementary material document. In summary, for each problem we can formulate the solution in terms of an integral equation for an unknown vertical velocity across the horizontal gap aligned with the lower edge of the floe. It turns out that this integral equation always has the same kernel, $T(x, x')$, as defined by (3.13) and therefore the main difference is that the right-hand side forcing term differs according to the problem being solved. This can be traced back to the way each problem is set up: a bespoke particular solution is needed to account for the inhomogeneous boundary conditions associated with the imposed velocity on the sides of the rectangular floe in different modes of motion. The other main difference is that the formulae that define the hydrodynamic forces vary since these also depend upon the particular solution. The details do become complicated particularly when we consider pitch motions and pitch-induced hydrodynamic forces since the imposed conditions on the boundary have components in both domains V^+ and V^- .

The method for producing numerical approximations is also similar to what has been described previously and details are given in the supplementary material.

In the remaining part of the paper we concentrate on the explicit approximations derived for small gaps assuming frequencies that are away from resonance, which is the main range of interest for the application area in mind: the low frequency wave propagation through broken ice.

4.1 Surge constrained motions for small gaps

From the solution of the surge problem we are able to determine the leading order approximation to the surge-induced surge component of the force in terms of the dimensionless gap size ϵ as

$$F^{(s,s)} \approx \frac{1}{\epsilon} \frac{4\hat{\rho}^2}{KL} \sin^2\left(\frac{kL}{2}\right) \left(\frac{1}{3} K\hat{\rho}d - 1 - \frac{(K\hat{\rho}d - 2)^2}{4(K\hat{\rho}d - 1) + 2\epsilon Kd \cot(kL/2)} \right). \quad (4.1)$$

(see equation (S.1.20) in the supplementary material). We may immediately consider surge-constrained motions by extracting from (2.15) the condition

$$F^{(s,s)} + \hat{\rho} = 0. \quad (4.2)$$

As this is clearly a transcendental equation, we may use a root-finding algorithm to find solutions—noting that we do not have the aforementioned issues as this form is only leading order.

When $kL \gg O(\epsilon)$ or $2\pi - kL \gg O(\epsilon)$, we note that $\cot(kL/2) = O(1)$ and we can neglect the $O(1)$ term $\cot(kL/2)$ in (4.1), simplifying it to

$$F^{(s,s)} \approx \frac{1}{\epsilon} \frac{\hat{\rho}^3 d (4 - K\hat{\rho}d)}{3L(1 - K\hat{\rho}d)} \sin^2\left(\frac{kL}{2}\right) \quad (4.3)$$

resulting in the dispersion relation

$$\sin^2\left(\frac{kL}{2}\right) \approx \epsilon \frac{3L(1 - K\hat{\rho}d)}{\hat{\rho}^2 d (K\hat{\rho}d - 4)} \quad (4.4)$$

which is 2π -periodic in kL . This reduction is useful since it shows from (4.4) that solutions are predicted to exist for $1 \leq K\hat{\rho}d \leq 4$ and that there is symmetry in kL about π in the surge-only case.

The solution of (4.2) using (4.1) via root-finding results in the curves labelled in Fig. 3 as asymptotic results. They are shown to agree very well with the accurate full numerical results across all frequencies and improve as ϵ is reduced in size, as expected. As predicted, the dispersion curves fall mainly within the region $1 \leq K\hat{\rho}d \leq 4$. However, note the vital role that the extra term $\epsilon \cot(kL/2)$ in (4.1) has in allowing the asymptotically-derived results to follow the exact results beyond this range as kL tends to 0 and 2π as the aforementioned symmetry is broken. Since we are motivated by results at low frequencies, we note the importance of retaining the $\epsilon \cot(kL/2)$ term in (4.1).

4.2 Heave-surge coupled motions for small gaps

An asymptotic analysis for small gaps, away from resonance (see supplementary material), leads to the result

$$F^{(h,s)} = i\hat{\rho} \frac{\frac{1}{2}K\hat{\rho}d - 1}{K\hat{\rho}d - 1 + \frac{1}{2}\epsilon Kd \cot\left(\frac{kL}{2}\right)} = -F^{(s,h)} \quad (4.5)$$

confirming the reciprocal relation (2.17). Again, we note the inclusion of a term proportional to $\epsilon \cot(kL/2)$ originating from (3.35) which is $O(1)$ in the vicinity of $kL = 0$ and $kL = 2\pi$.

If the motion is constrained so that floes move freely in heave and surge without pitching then the last element of (2.15) is suppressed so that the motion is defined by the 2×2 upper-left system of equations and the dispersion relation is defined by

$$Kd \left(\hat{\rho} + F^{(s,s)} \right) \left(Kd \left(\hat{\rho} + F^{(h,h)} \right) - 1 \right) - \left| Kd F^{(h,s)} \right|^2 = 0. \quad (4.6)$$

We can make accurate numerical calculations of solutions of this dispersion relation using the numerical methods that define the hydrodynamic forces.

Assuming small gaps and using the expressions (3.41), (3.42) (4.1) and (4.5), we see that all forces are $O(1)$ except for $F^{(s,s)} = O(1/\epsilon)$ and thus it is clear that, at leading order, (4.6) reduces to

$$F_0^{(h,h)} \approx \frac{1 - K\hat{\rho}d}{Kd} \quad (4.7)$$

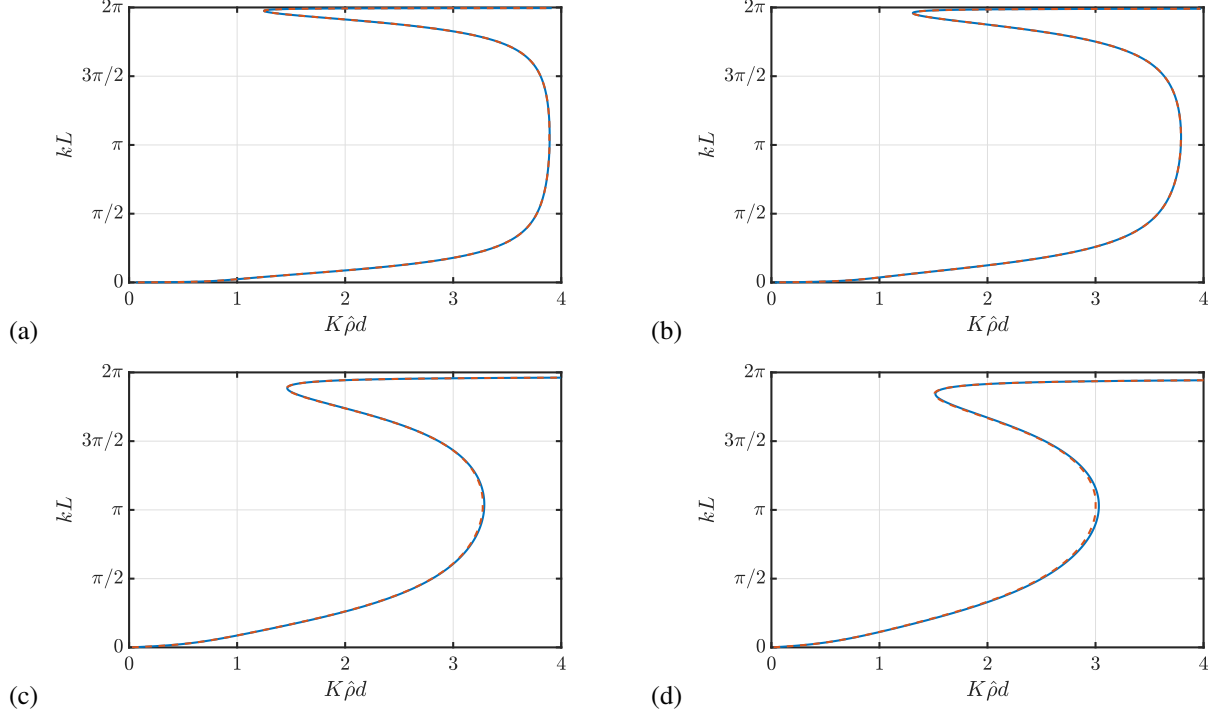


Figure 3: Dispersion curves (kL versus $K\hat{\rho}d$) for surge-constrained motions in the case $\hat{\rho} = 0.9$, $L/d = 1 + \epsilon$ (square ice floes). Exact results (blue solid curves) and small-gap approximations (orange, dashed) for gap sizes: (a) $\epsilon = 0.01$, (b) $\epsilon = 0.02$, (c) $\epsilon = 0.08$, (d) $\epsilon = 0.12$.

which is the leading-order approximation corresponding to heave-constrained motion. That is, solutions of (4.7) are just

$$k \approx \frac{2}{L} \cot^{-1} \left(\frac{2(1 - K\hat{\rho}d)}{KL} \right) \quad (4.8)$$

the same as (3.44). This is perhaps not surprising since as the gaps shrink, the effect of surge is reduced. Since we only have leading order estimates for the forces $F^{(s,h)}$ and $F^{(s,s)}$ (unlike for $F^{(h,h)}$) we are unable to perform a consistent expansion of (4.6) in higher order powers of ϵ that allows us to deduce an improved explicit estimate of k dependent upon ϵ as we did in the heave- and surge-constrained cases.

Instead, Fig. 4 shows a comparison of the full numerical solutions of the coupled heave-surge motions alongside curves calculated from using the small gap approximations (3.40), (3.41), (4.1) and (4.5) in (4.6) with increasing values of ϵ for the same square floe configuration used in the previous results.

In the low frequency region $K\hat{\rho}d < 1$ exact results correspond closely to the heave-constrained approximation consistent with the result (4.8). The influence of gap resonance and standing wave solutions on the results using the leading-order asymptotic theory are significant as ϵ moves away from zero. Additional solution branches, not associated with exact solutions, emerge from the narrow strips in the dispersion diagram where the analysis is invalid, exaggerated, perhaps, because of the 2π -periodicity constraint on solutions.

4.3 Pitch constrained motions for small gaps

We consider floe motions which are constrained to the pitching mode only (i.e. the heave/surge is suppressed). According to (2.15) the condition for such modes to exist is

$$\frac{1}{12} - \frac{1}{2}\hat{\rho}(1 - \hat{\rho})d^2 - \frac{1}{12}K\hat{\rho}d(1 + d^2) - KdF^{(p,p)} = 0. \quad (4.9)$$

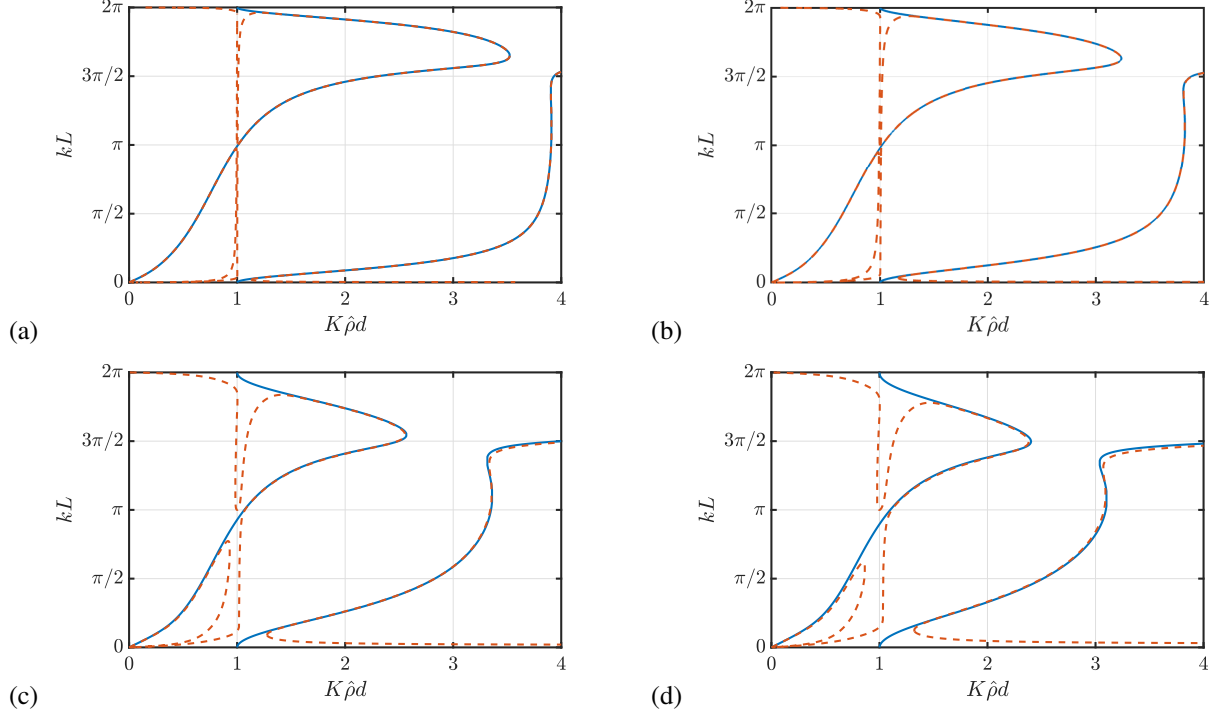


Figure 4: Dispersion curves (kL versus $K\hat{\rho}d$) for heave and surge-constrained motions in the case $\hat{\rho} = 0.9$, $L/d = 1 + \epsilon$ (square ice floes). Exact results (blue solid curves) and small-gap approximations (orange, dashed) for gap sizes: (a) $\epsilon = 0.01$, (b) $\epsilon = 0.02$, (c) $\epsilon = 0.08$, (d) $\epsilon = 0.12$.

For small gaps we can use the approximation

$$F^{(p,p)} = \frac{1}{\epsilon} \hat{\rho}^2 \left(\frac{d}{L}\right)^3 \left[\frac{\hat{\rho}^3}{5} - \frac{\hat{\rho}^2}{2} + \frac{\hat{\rho}}{3} - \frac{(1-\hat{\rho})^2}{Kd} - \frac{\left(\frac{\hat{\rho}^2}{3} - \frac{\hat{\rho}}{2} + \frac{1-\hat{\rho}}{Kd}\right)^2}{\frac{K\hat{\rho}d-1}{Kd} + \frac{1}{2}\epsilon \cot\left(\frac{kL}{2}\right)} \right] \sin^2\left(\frac{kL}{2}\right) \quad (4.10)$$

which is derived in the supplementary material. For values of kL not close to 0 or 2π we may neglect the $\epsilon \cot(kL/2)$ term, simplifying the above to

$$F^{(p,p)} \approx \frac{1}{\epsilon} \frac{d^3}{L^3} \hat{\rho}^2 \sin^2(kL/2) \left(\frac{Kd}{1-K\hat{\rho}d} \left(\frac{\hat{\rho}^2}{3} - \frac{\hat{\rho}}{2} + \frac{1-\hat{\rho}}{Kd} \right)^2 + \frac{\hat{\rho}^3}{5} - \frac{\hat{\rho}^2}{2} + \frac{\hat{\rho}}{3} - \frac{(1-\hat{\rho})^2}{Kd} \right). \quad (4.11)$$

It can be shown from (4.11) that as $Kd \rightarrow 0$

$$F^{(p,p)} \rightarrow \frac{1}{\epsilon} \frac{d^3}{L^3} \left(\frac{28}{15} \hat{\rho}^3 - \frac{25}{6} \hat{\rho}^2 + \frac{7}{3} \hat{\rho} \right) \sin^2(kL/2). \quad (4.12)$$

That is, terms proportional to $1/Kd$ in (4.11) cancel. As a result there can be no solutions, kL , to (4.9) in the zero frequency limit away from $(0,0)$. However, we note that for small ϵ , (4.9) has solutions, kL , for values of Kd in proportion to ϵ . This means that as $\epsilon \rightarrow 0$, solutions exist as $Kd \rightarrow 0$. This behaviour can be observed in the dispersion diagram of Fig. 5, there being a low-frequency branch of solutions running from $kL = 0$ to $kL = 2\pi$. The small-gap approximation without the $\epsilon \cot(kL/2)$ term defined by (4.11) is symmetric with respect to $kL = \pi$ when used in (4.9). The exact results are not symmetric, as shown in Fig. 5, once again showing the value of including the additional term. The comments made about surge motion close to $kL = 0, 2\pi$ apply here also. The importance of the $\epsilon \cot(kL/2)$ term in (4.10) in computing the small-gap approximation is evident in Fig. 6 where (4.10) with (4.9) are shown to produce accurate approximations in all cases.

To further illustrate the interaction between different modes we briefly consider the effect of coupling pitch to heave and surge motions. As with coupled heave-surge motion previously, this means selectively restricting (2.15) to the

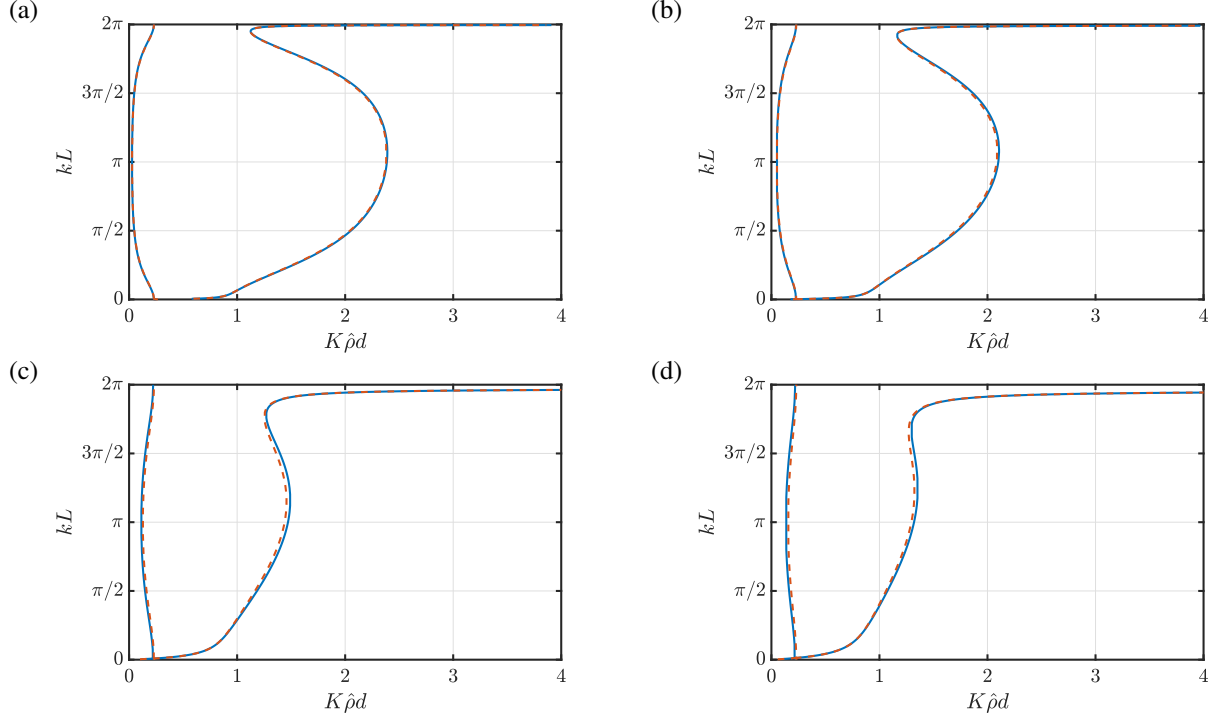


Figure 5: Dispersion curves (kL versus $K\hat{\rho}d$) for pitch-constrained motions in the case $\hat{\rho} = 0.9$, $L/d = 1 + \epsilon$ (square ice floes). Exact results (blue solid curves) and small-gap approximations (orange, dashed) for gap sizes: (a) $\epsilon = 0.01$, (b) $\epsilon = 0.02$, (c) $\epsilon = 0.08$, (d) $\epsilon = 0.12$.

appropriate 2×2 subsystem. When small gaps are assumed, we use the approximation (see supplementary material)

$$F^{(h,p)} = i \left(\frac{L}{12d} + \frac{\hat{\rho}d}{2L} \frac{\frac{\hat{\rho}^2}{3} - \frac{\hat{\rho}}{2} + \frac{1-\hat{\rho}}{Kd}}{\frac{K\hat{\rho}d-1}{Kd} + \frac{1}{2}\epsilon \cot\left(\frac{kL}{2}\right)} \right) = -F^{(p,h)}. \quad (4.13)$$

In Fig. 6 we show the dispersion curves for motions constrained to pitch/heave motions, i.e. surge motion is suppressed. Exact computations are shown against approximations for small gaps. We see a superposition of the effects seen in Figs. 2 and 5. The low-frequency branch from the pitch-constrained solution exists alongside the heave-constrained mass-loading curve, but we note that it is not simply a superposition of heave and pitch. The heave resonance that manifests as an asymptote at $K\hat{\rho}d = 1$ in the heave-constrained is suppressed when heave is coupled with either surge, pitch or both. Instead, exact results follow the leading-order heave solution in these coupled cases. Beyond low frequencies, we see similar effects to those observed for coupled heave-surge motions in relation to how approximate solutions diverge from the exact counterparts as frequencies tend to resonance ($K\hat{\rho}d = 1$) or wave motion tends to standing waves ($kL = 0, 2\pi$). The distortions to approximate solutions that are constrained to be 2π -periodic in kL lead to the emergence of solution branches which are not associated with exact solutions.

The same general observations can be made regarding Fig. 7, where we consider pitch/surge coupled motions. In the previous results where two modes have been coupled (heave/surge in Fig. 4 and heave/pitch in Fig. 6) the resulting dispersion diagrams have, to a good approximation, appeared as a superposition of the two sets of dispersion curves from each component mode. In Fig. 7 we see that the dispersion curves are related to those in Figs. 3 and 5. However, only the low frequency branch of the pitch mode is represented in Fig. 7 and the branch which extends into $K\hat{\rho}d > 1$ is missing. We cannot determine a physical or mathematical reason for why this might be. It is worth remarking that the results obtained using the asymptotic results for coupled surge/pitch motions match the exact results well across all frequencies. That is, there appears to be no issue with frequencies close to resonance, as experienced in the results involving coupling with heave.

Here, the small-gap approximation is derived in the supplementary material to be

$$F^{(s,p)} = \frac{1}{\epsilon} \frac{\hat{\rho}^2 d}{KL^2} \left(2Kd \left(\frac{\hat{\rho}^2}{4} - \frac{\hat{\rho}}{3} + \frac{1-\hat{\rho}}{Kd} \right) - \frac{K\hat{\rho}d-2}{\frac{K\hat{\rho}d-1}{Kd} + \frac{1}{2}\epsilon \cot\left(\frac{kL}{2}\right)} \left(\frac{\hat{\rho}^2}{3} - \frac{\hat{\rho}}{2} + \frac{1-\hat{\rho}}{Kd} \right) \right) \sin^2\left(\frac{kL}{2}\right) \quad (4.14)$$

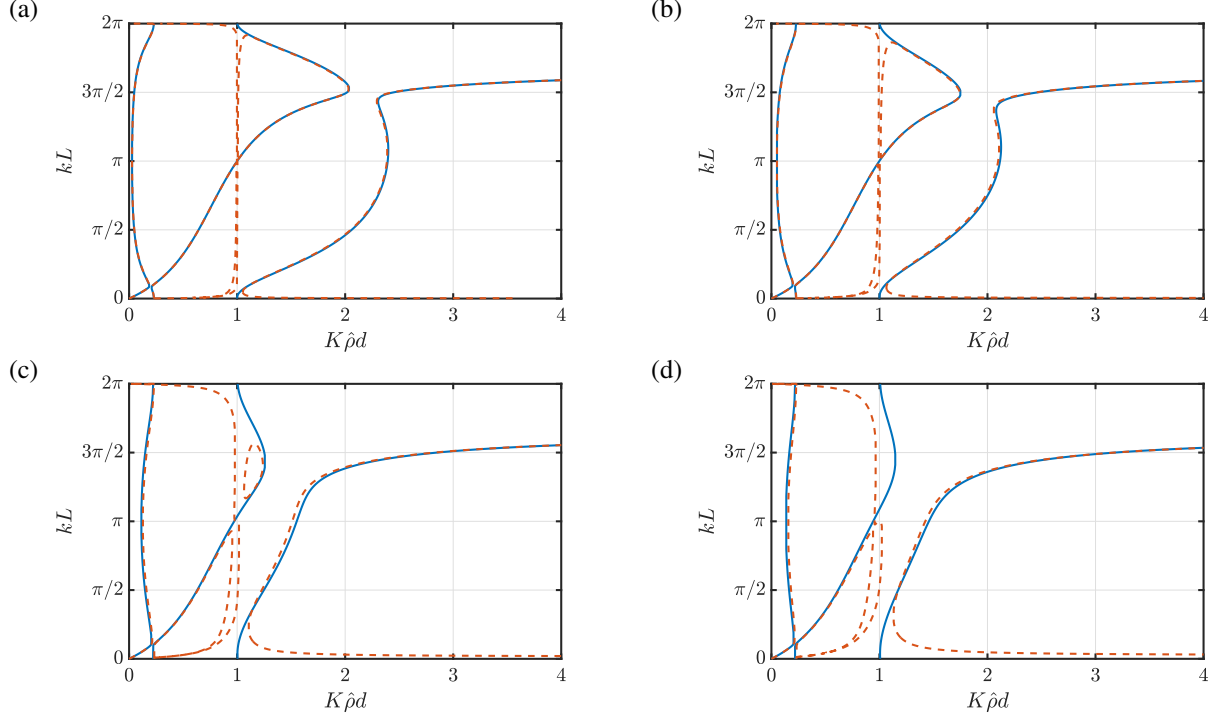


Figure 6: Dispersion curves (kL versus $K\hat{\rho}d$) for heave/pitch-constrained motions in the case $\hat{\rho} = 0.9$, $L/d = 1 + \epsilon$ (square ice floes). Exact results (blue solid curves) and small-gap approximations (orange, dashed) for gap sizes: (a) $\epsilon = 0.01$, (b) $\epsilon = 0.02$, (c) $\epsilon = 0.08$, (d) $\epsilon = 0.12$.

5 Fully unconstrained problem

The fully unconstrained problem treats the rectangular floe as a rigid body free to heave, surge and pitch. The dispersion relation is expressed by the vanishing of the 3×3 determinant in (2.15), coupling all three rigid-body modes. Numerical solutions are obtained using the Galerkin method described in Section 3, extended to include the surge and pitch subproblems. Approximate solutions for small gaps use the asymptotic force expressions derived in the preceding sections.

We now consider results for the problem originally conceived in this paper whereby waves propagate through freely-floating rectangular floes. The previous sets of results which describe relations between frequency and wavenumber for motions which are constrained to move in either one mode or two coupled modes have been useful in establishing certain fundamental features associated with heave, surge and pitch motions. In particular we can observe that when two modes are coupled, the resulting dispersion diagrams are, to a large extent, a superposition of the dispersion curves for the two uncoupled modes. Where two single mode curves intersect, the coupling creates connecting loops characteristic of saddle points. These features are most clear to see when the gaps between floes are small. Increasing the size of the gaps between floes strengthens the coupling, distorting the dispersion curves further away from the superposition of the two component dispersion curves. The exceptions have been in the coupling of surge and pitch, which has resulted in one of the component branches being dropped from the combined dispersion diagram; and heave, when coupled to either surge or pitch, suppresses the heave-constrained asymptote at resonance in the exact results, although the asymptotic small-gap results do not suppress this effect.

In Fig. 8 we show the dispersion diagram for unconstrained motion (freely-floating floes) corresponding to the same array of square floes and gaps that have been the subject of Figs. 2–7. Again, the solid blue curves represent the

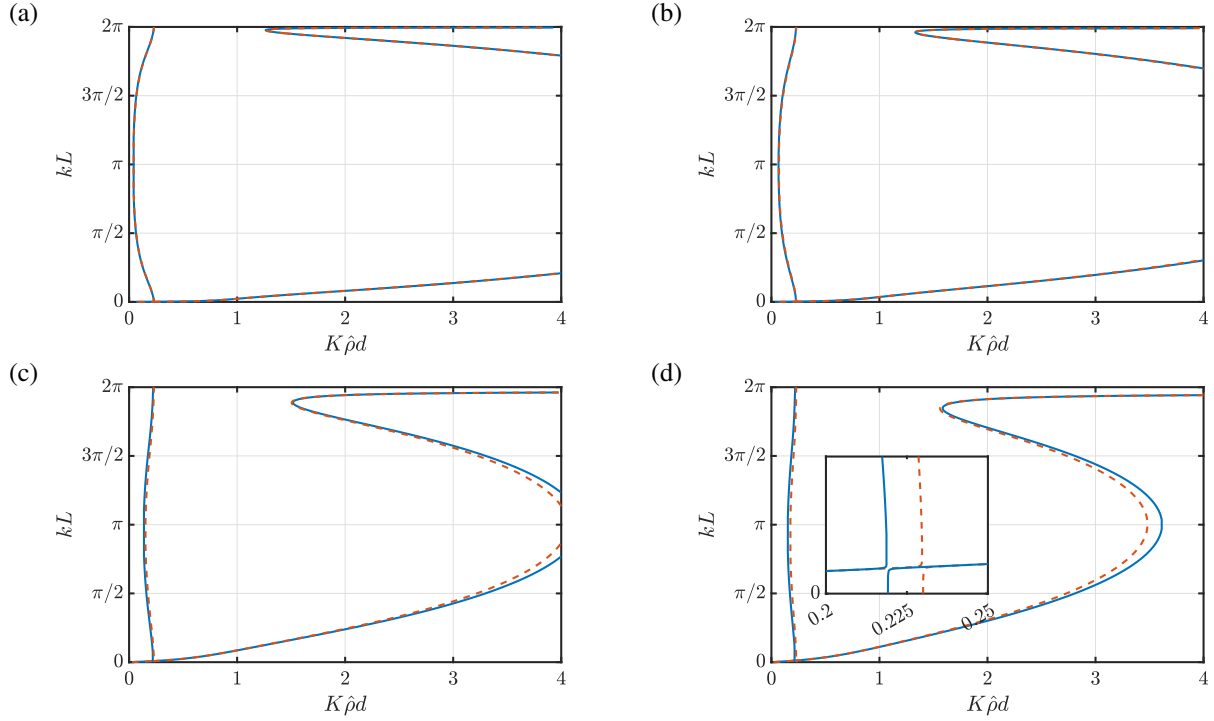


Figure 7: Dispersion curves (kL versus $K\hat{\rho}d$) for surge/pitch-constrained motions in the case $\hat{\rho} = 0.9$, $L/d = 1 + \epsilon$ (square ice floes). Exact results (blue solid curves) and small-gap approximations (orange, dashed) for gap sizes: (a) $\epsilon = 0.01$, (b) $\epsilon = 0.02$, (c) $\epsilon = 0.08$, (d) $\epsilon = 0.12$.

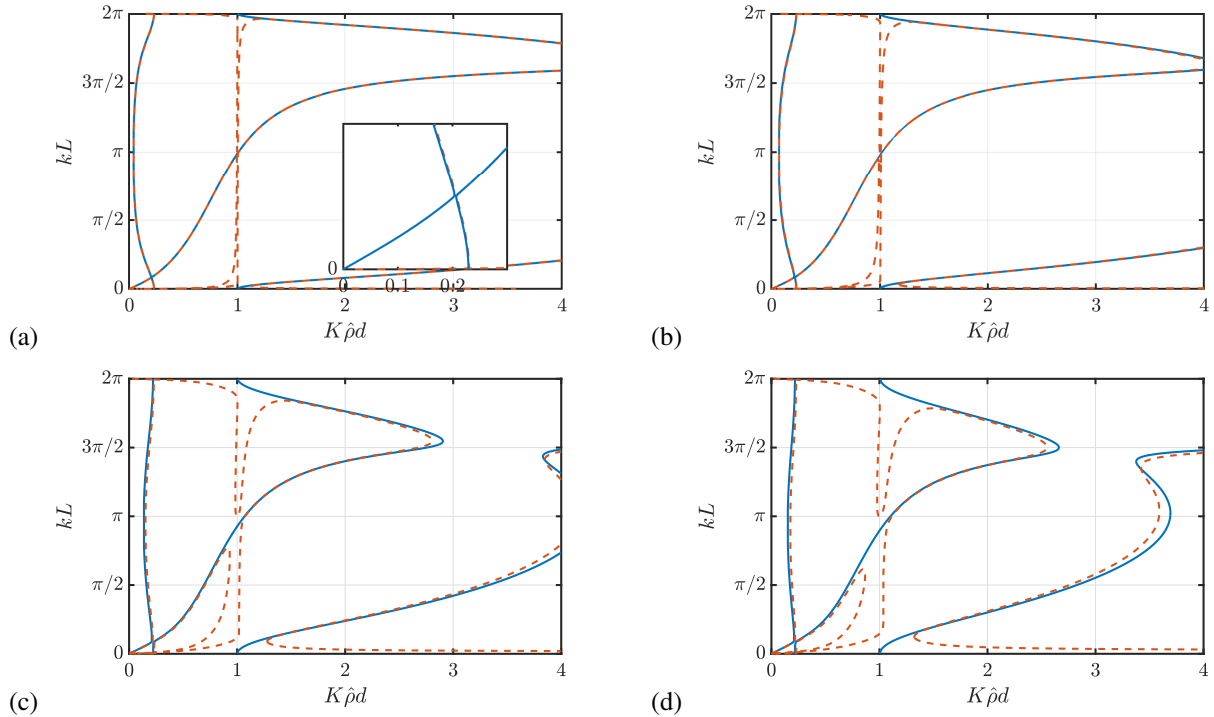


Figure 8: Dispersion curves (kL versus $K\hat{\rho}d$) for fully unconstrained motions in the case $\hat{\rho} = 0.9$, $L/d = 1 + \epsilon$ (square ice floes). Exact results (blue solid curves) and small-gap approximations (orange, dashed) for gap sizes: (a) $\epsilon = 0.01$ with low-frequency results inset, (b) $\epsilon = 0.02$, (c) $\epsilon = 0.08$, (d) $\epsilon = 0.12$.

numerical solutions based on the exact method and the orange dashed curves correspond to approximate solutions that have used the asymptotic results for each of the component hydrodynamic forces (that is, the definitions (3.40), (3.41), (4.1), (4.5), (4.11), (4.14) have been used in (2.15)).

The combined dispersion diagram in Fig. 8 combines curves from each component heave, surge and pitch modes as we might expect from our analysis of the previous sets of results. Thus, only the low-frequency branch of the pitch dispersion curve is represented in Fig. 8 and the branch that extends into $K\hat{\rho}d > 1$ is missing from Fig. 8, as it was from the combined surge/pitch results in Fig. 7; the heave resonance is also suppressed. The approximations obtained from the asymptotic evaluations of the forces under the small-gap approximation are generally good apart from close to resonance, $K\hat{\rho}d = 1$.

The intended purpose of this work relates to low frequency wave propagation, well below $K\hat{\rho}d = 1$, and here we can see that the small-gap results capture quite accurately the low frequency dispersion curves. The dominant branch extending away from $(0, 0)$ in the dispersion diagrams in Fig. 8 follows very closely the curves in Fig. 2 based on heave-constrained motion. What is surprising in these results is the existence of a low-frequency branch representing pitch-constrained motions.

In Figs. 9, 10 and 11 we consider the effect that changing the aspect ratio of the floes has on the results for unconstrained motions (that is, we make no detailed analysis of the constrained components as we have done for square floes). We can see that as the floes become longer, the low-frequency branch associated with pitch moves towards higher frequencies (though still below $K\hat{\rho}d = 1$). In particular, since $F^{(p,p)}$ in (4.10) is proportional to $(d/L)^3$, pitch effects become increasingly suppressed as the aspect ratio grows. For the 4:1 aspect ratio the pitch-dominated branch is barely visible in the low-frequency regime and the dispersion diagram is dominated by the heave mode. The saddle point-like bifurcation at the intersection of heave and pitch branches that is clearly visible for square floes coalesces to form a single branch as the aspect ratio increases. This branch initially follows the heave-constrained dispersion relation before becoming a pitch-dominant mode.

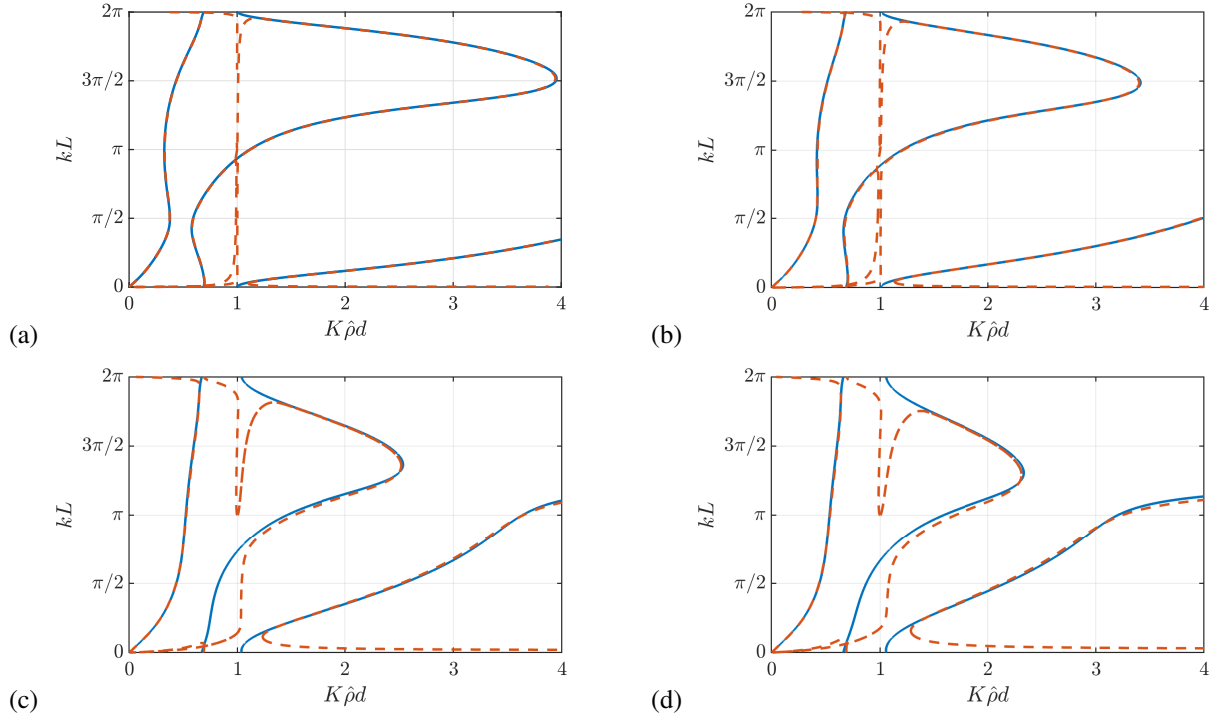


Figure 9: Dispersion curves (kL versus $K\hat{\rho}d$) for fully unconstrained motions in the case $\hat{\rho} = 0.9$, $L/d = 2 + \epsilon$ (2:1 aspect ratio floes). Exact results (blue solid curves) and small-gap approximations (orange, dashed) for gap sizes: (a) $\epsilon = 0.01$, (b) $\epsilon = 0.02$, (c) $\epsilon = 0.08$, (d) $\epsilon = 0.12$.

In Fig. 12 we focus on the low-frequency regime ($0 < K\hat{\rho}d < 0.5$) for $\epsilon = 0.08$ across the four aspect ratios. Here, the leading-order heave approximation (orange, dashed) is compared alongside the mass-loading solution of Dafydd and Porter (2026) (purple, dot-dashed). The mass-loading dispersion relation is accurate for all values of L/d considered, which is surprising given that the leading-order heave solution fails to describe it as accurately. In fact, we expect the

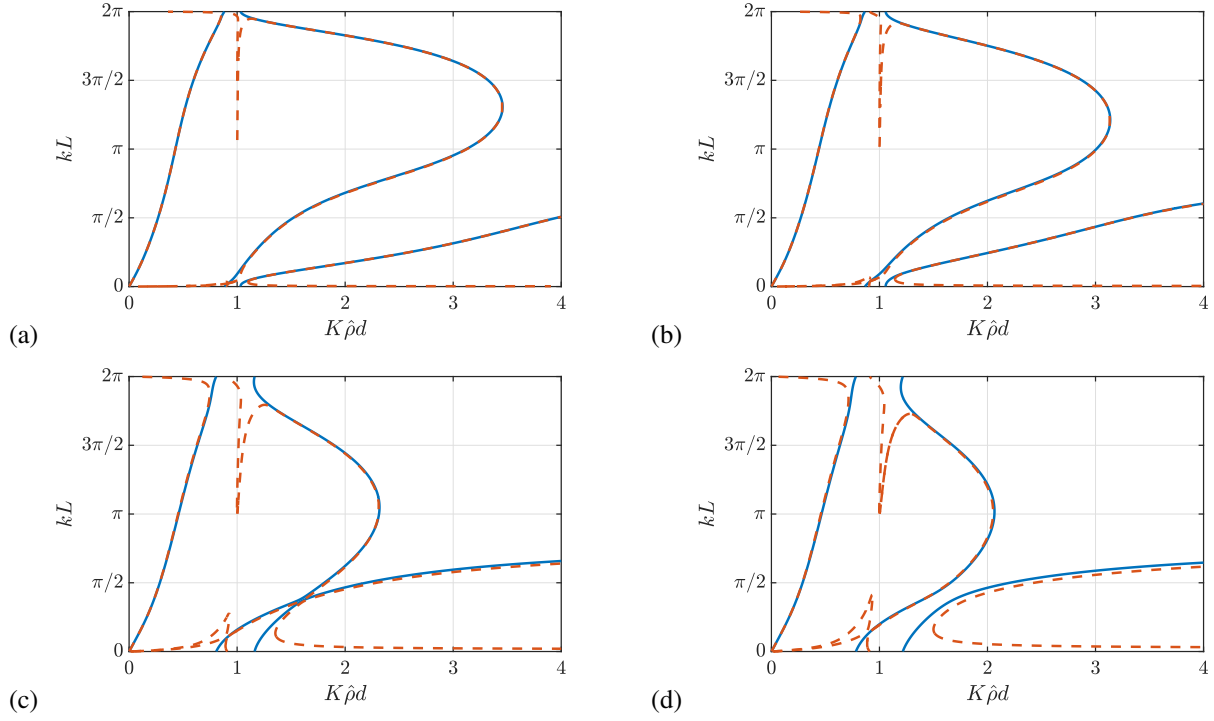


Figure 10: Dispersion curves (kL versus $K\hat{\rho}d$) for fully unconstrained motions in the case $\hat{\rho} = 0.9$, $L/d = 4 + \epsilon$ (4:1 aspect ratio floes). Exact results (blue solid curves) and small-gap approximations (orange, dashed) for gap sizes: (a) $\epsilon = 0.01$, (b) $\epsilon = 0.02$, (c) $\epsilon = 0.08$, (d) $\epsilon = 0.12$.

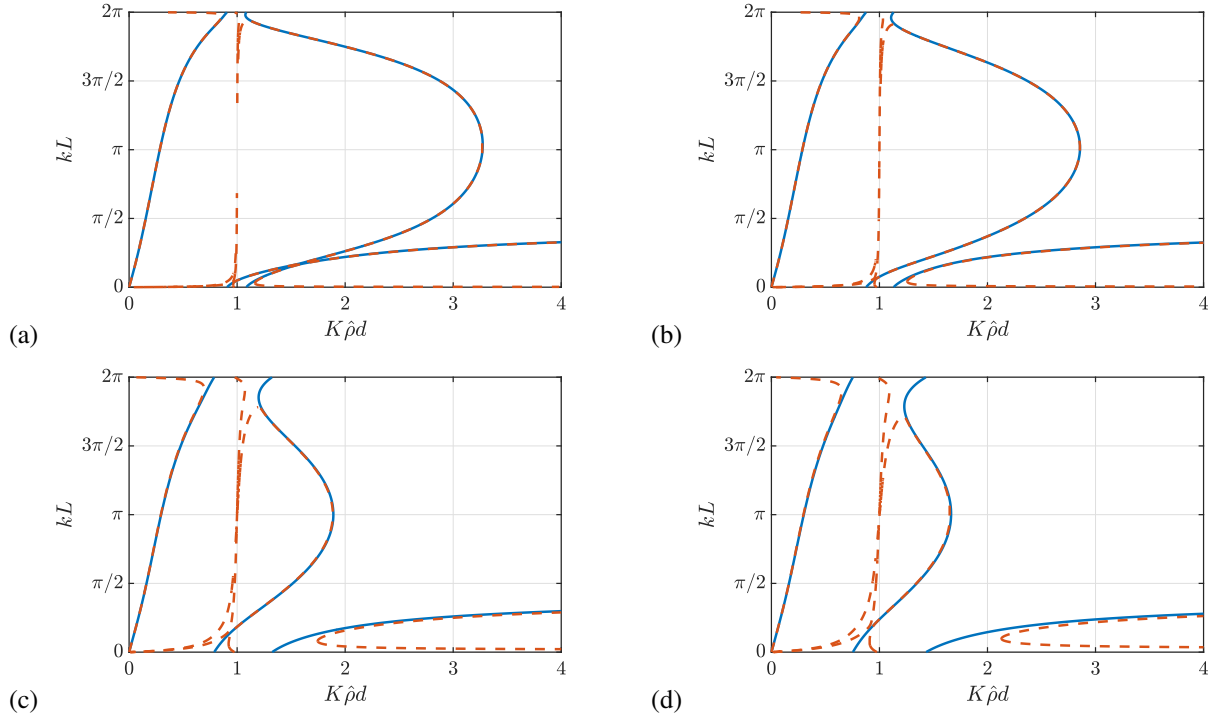


Figure 11: Dispersion curves (kL versus $K\hat{\rho}d$) for fully unconstrained motions in the case $\hat{\rho} = 0.9$, $L/d = 8 + \epsilon$ (8:1 aspect ratio floes). Exact results (blue solid curves) and small-gap approximations (orange, dashed) for gap sizes: (a) $\epsilon = 0.01$, (b) $\epsilon = 0.02$, (c) $\epsilon = 0.08$, (d) $\epsilon = 0.12$.

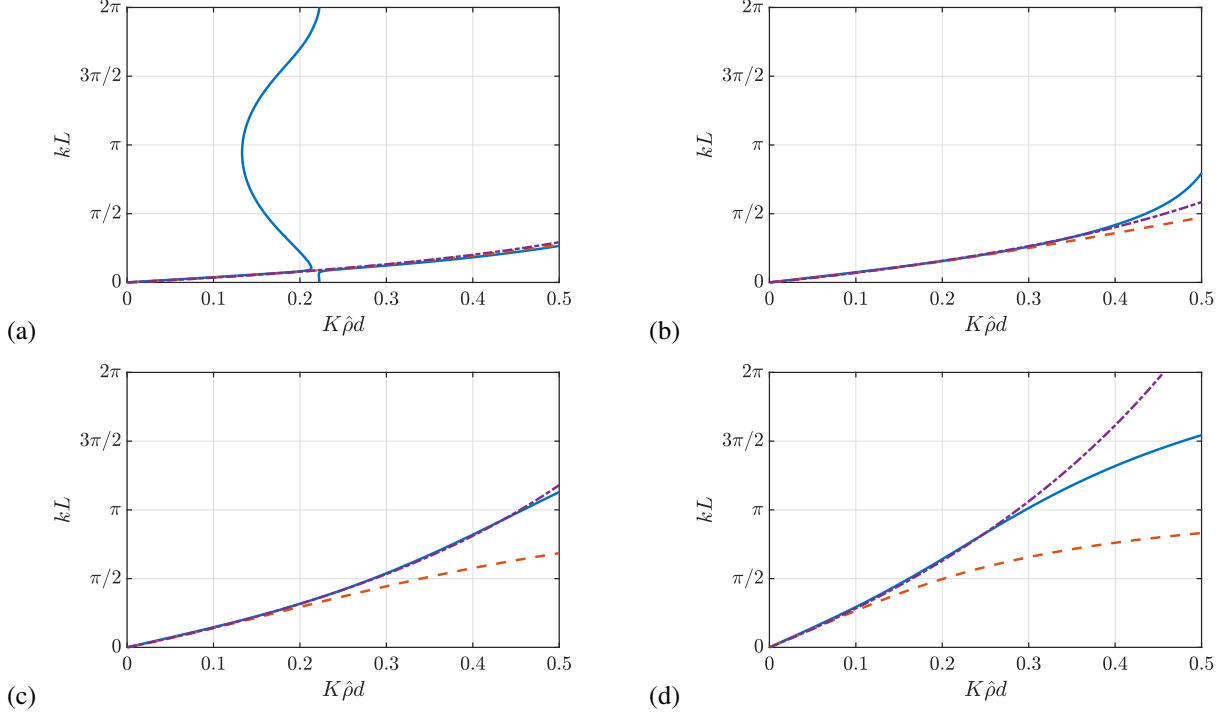


Figure 12: Low-frequency dispersion curves (kL versus $K\hat{\rho}d$ for $0 < K\hat{\rho}d < 0.5$) for fully unconstrained motions in the case $\hat{\rho} = 0.9$ and $\epsilon = 0.08$. Exact results (blue solid curves), leading-order heave approximation (orange, dashed) and mass-loading solution of Dafydd and Porter (2026) (purple, dot-dashed) for aspect ratios: (a) $L/d = 1 + \epsilon$, (b) $L/d = 2 + \epsilon$, (c) $L/d = 4 + \epsilon$, (d) $L/d = 8 + \epsilon$.

leading-order asymptotic heave solution to fail as terms proportional to L/d become dominant and terms proportional to d/L get small, resulting in the leading-order behaviour of the asymptotics no longer being concretely described by the leading-order heave solution.

Here we find Fig. 13 useful. In Fig. 13(a) we have reproduced the dispersion diagram of Fig. 9 corresponding to $\epsilon = 0.12$ using R-G-B colour coding to represent the relative amplitude of (respectively) the heave-surge-pitch motions. The normalised amplitudes of each mode are displayed on individual plots in Figs. 13(b,c,d) with the same colour coding. Thus, we can determine that the low-frequency dispersion curve which approximately follows the heave-constrained curve for small $K\hat{\rho}d$ is not simply heave motion, but a roughly equal combination of heave and surge motion. Furthermore, these two motions are a quarter of a period out of phase with one another and thus the motion along this low-frequency branch is actually circular floe motion, even though the dispersion relation is approximately that satisfied by constrained heave motion.

Further along this branch we see that pitch becomes increasingly dominant. At a particular frequency corresponding to $kL = 2\pi$ the motion is entirely pitch; each floe is now pitching in phase with its neighbours at a frequency some way below the resonant frequency of the fluid in the narrow channel. We can also see that for an interval of frequency, just above $K\hat{\rho}d = 1$ corresponding to fluid resonance and extending to roughly $K\hat{\rho}d = 2.3$, three possible propagating wave modes are now possible. Each one has its own frequency-dependent blend of heave, surge and pitch components.

The solution landscape is evidently remarkably rich and complicated and hard to understand physically. To help in developing some understanding, in Fig. 14(a–g) we have plotted sample snapshots in time of the floe motion corresponding to various points in the corresponding dispersion diagram. Much more useful is the online tool (see Dafydd (2026)) that we have developed which provides time-varying simulations of fluid/floe motion and the user can pick any point they choose within the dispersion diagram, not just the seven used to produce Fig. 14.

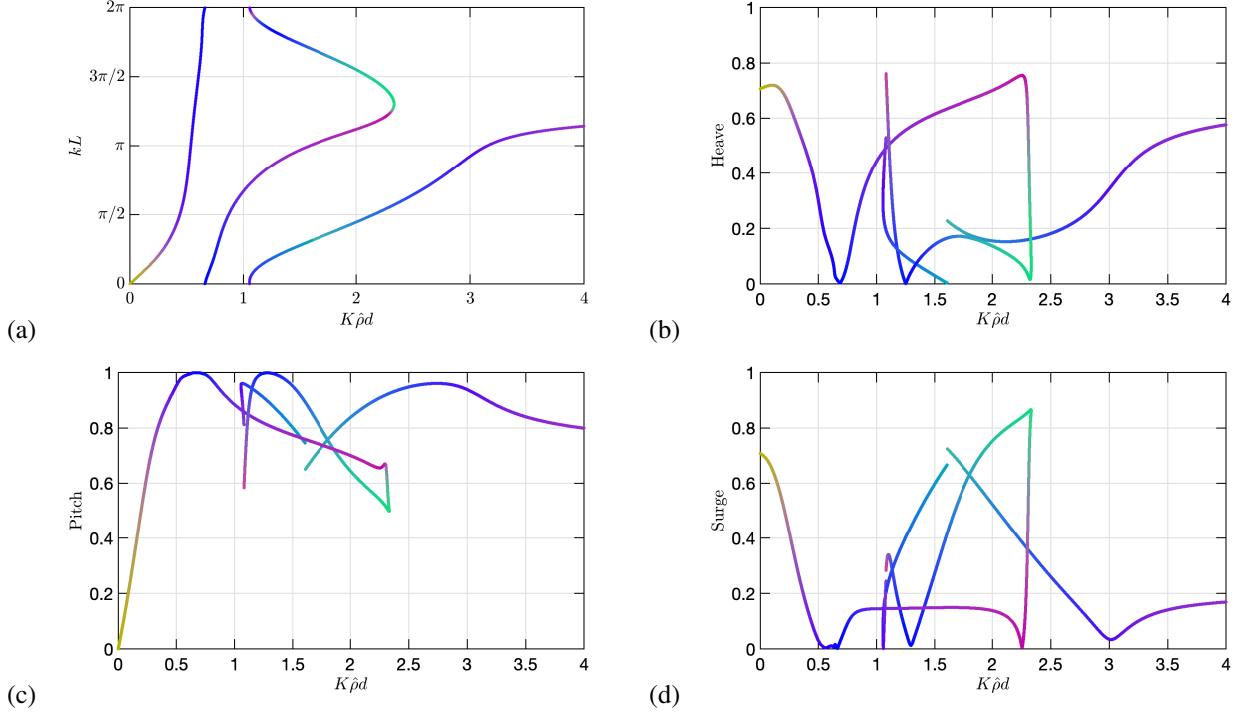


Figure 13: Colour coded plots of the heave-surge-pitch model for $\epsilon = 0.12$, $L/d = 2 + \epsilon$, $\hat{\rho} = 0.9$. (a) Wavenumber plot, (b) absolute heave value, (c) absolute surge value, (d) absolute pitch value.

6 Conclusions

The central question of this paper was to determine whether the heave-only, zero-gap model used by Dafydd and Porter (2024, 2026) provides a reasonable approximation to wave propagation through an array of freely-floating floes separated by small gaps. We address this question here.

In the low-frequency regime, which is the range of primary interest for the application to wave propagation through broken ice, the heave-constrained zero-gap dispersion relation does indeed provide a good approximation to the dispersion relation for freely-floating floes with small gaps. For all cases considered in this paper, the dominant low-frequency branch extending from $(kL, K\hat{\rho}d) = (0, 0)$ in the fully unconstrained results (Fig. 8) follows very closely the heave-constrained mass-loading curve of Dafydd and Porter (2026). The close agreement persists for floes with larger aspect ratios (Figs. 9, 10, 11).

However, the situation is more nuanced than the dispersion relation alone suggests. An examination of the modal amplitudes (Fig. 13) reveals that along this dominant low-frequency branch, the floe motion is not simply heave: it is a roughly equal combination of heave and surge with a quarter-period phase shift between the two components, producing a circular floe motion. Thus, even though the dispersion relation is well approximated by the heave-only model, the actual floe kinematics are fundamentally different.

A further complication arises from the pitch mode. For floes of small aspect ratio (we have shown results for square floes, or $d/(L - \ell) = 1$), a low-frequency pitch-dominated branch of solutions co-exists alongside the heave-dominated curve (see Figs. 5, 8). Since $F^{(p,p)}$ in (4.10) is proportional to $(d/L)^3$, pitch effects are suppressed as the aspect ratio grows. For floes with aspect ratio 4:1, the pitch branch is shifted to higher frequencies and is far less prominent. However, for the small aspect-ratio floes assumed in Dafydd and Porter (2024, 2026), the pitch-dominated branch lies firmly within the low-frequency regime and represents an additional mode of wave propagation not captured by the heave-only model. It is unclear at this stage how multi-modal wave propagation would be incorporated into the ensemble-averaged multiple-scattering framework of Dafydd and Porter (2024, 2026), but it could potentially alter their theoretical prediction of wave attenuation. It should be noted that the leading order heave solution of Fig. 2 is shown to be increasingly poor at modeling the low-frequency branch of an unconstrained system in Fig. 14 as aspect ratios increase due to d/L becoming $O(\epsilon)$ or smaller and changing the balance of (2.15), but the mass-loading model remains surprisingly accurate throughout.

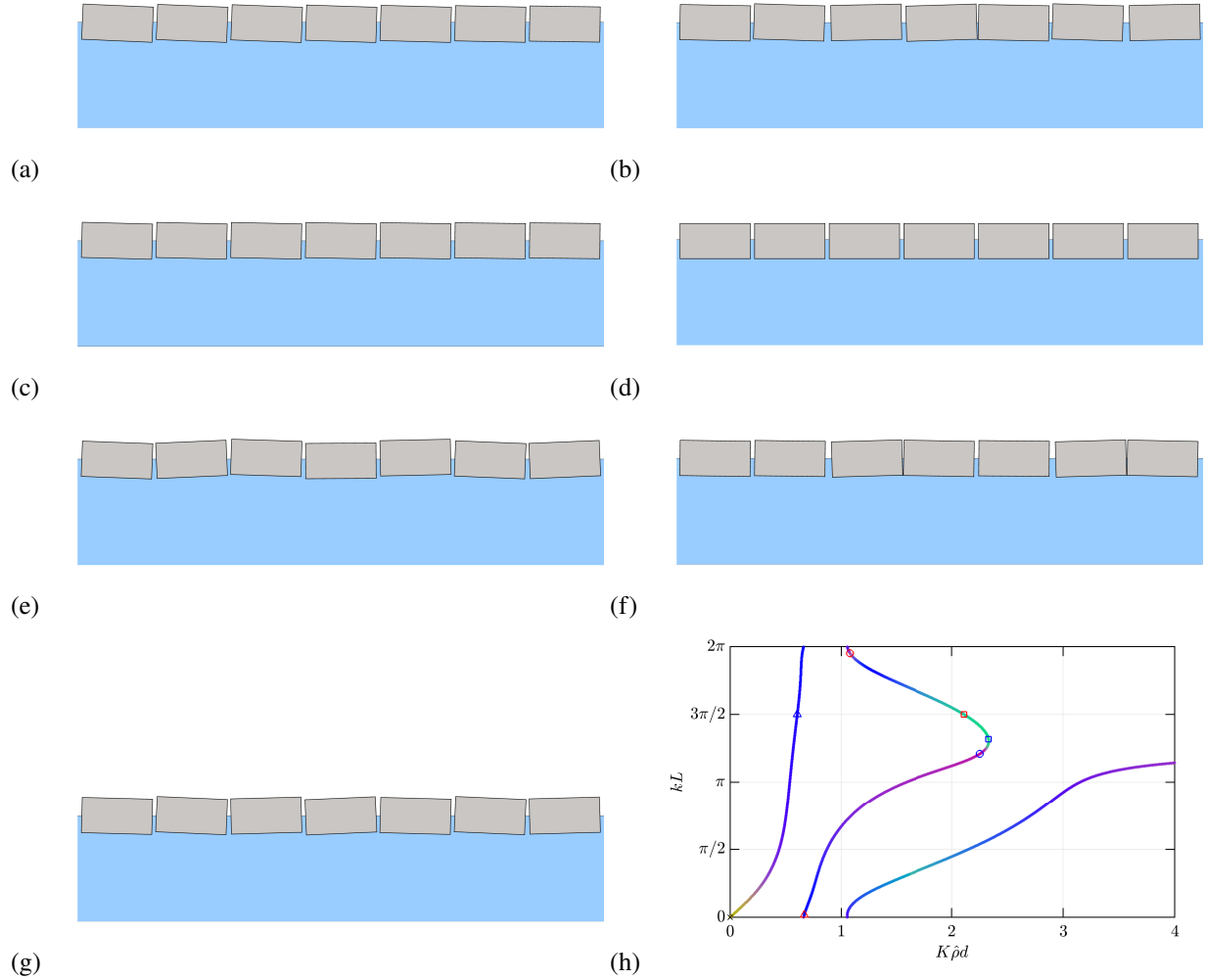


Figure 14: Representative snapshots at time $t = 2\pi/3$ from the seven animations together with the scatter plot that locates each snapshot in $(K\rho d, kL)$ space. (a), (b), (c): the most heave-, surge- and pitch-dominant in-phase modes. (d): the point closest to the origin. (e), (f), (g): the most heave-, surge- and pitch-dominant out-of-phase modes. (h) the scatter plot showing each point's spectral coordinates where blue represents in-phase, red represents out-of-phase and circles, squares and triangles represent heave-, surge- and pitch-dominant modes respectively. The black cross denotes the point chosen near the origin.

The small-gap asymptotic formulae developed in this paper provide computationally efficient approximations to the dispersion relation. Away from the narrow-channel resonance ($K\hat{\rho}d \neq 1$) and for kL not close to 0 or 2π , the leading-order expressions reproduce the numerical results well and reduce to the heave-constrained result at leading order when the motions are coupled. Close to resonance, the asymptotic expansion breaks down and the full numerical solution is required to capture the strong modal interactions.

Possible extensions of this work include the introduction of finite-depth effects, which will alter the positions and widths of the channel resonances, and the extension to three-dimensional floes to assess the role of roll and other out-of-plane motions on the modal structure.

References

- A. Allaire. Homogenization and two-scale convergence. *SIAM J. Math. Anal.*, 23:1482–1518, 1992.
- B. G. Carter and P. McIver. Water-wave propagation through an infinite array of floating structures. *J. Eng. Math.*, 81:9–45, 2013.
- T. Chou. Band structure of surface flexural-gravity waves along periodic interfaces. *J. Fluid Mech.*, 369:333–350, 1998.
- L. Dafydd and R. Porter. Attenuation of long waves through regions of irregular floating ice and bathymetry. *J. Fluid Mech.*, 996:A43, 2024.
- L. Dafydd and R. Porter. On the attenuation of waves through broken ice of randomly-varying thickness on water of finite depth. Submitted for publication, 2026.
- Lloyd Dafydd. *Wave-floe Response Visualiser*, 2026. URL <https://lloyd Dafydd.github.io/fffWebapp/>.
- A. G. Davies and A. D. Heathershaw. Surface-wave propagation over sinusoidally varying topography. *J. Fluid Mech.*, 144:419–443, 1984.
- G. S. Dias and J. H. Videman. Trapped modes along a periodic array of freely floating obstacles. *Math. Meth. Appl. Sci.*, 38:4038–4051, 2014.
- M. J. Doble, G. De Carolis, M. H. Meylan, J.-R. Bidlot, and P. Wadhams. Relating wave attenuation to pancake ice thickness, using field measurements and model results. *Geophys. Res. Lett.*, 42:4473–4481, 2015.
- D. V. Evans and M. Fernyhough. Edge waves along periodic coastlines. part 2. *J. Fluid Mech.*, 297:307–325, 1995.
- I. S. Gradshteyn and I. M. Ryzhik. *Table of integrals, series, and products*. Academic Press, Waltham, MA, 1981.
- L. Hošeková, M. P. Malila, W. E. Rogers, L. A. Roach, E. Eidam, and L. Rainville. Attenuation of ocean surface waves in pancake and frazil sea ice along the coast of the chukchi sea. *J. Geophys. Res.: Oceans*, 125:e2020JC016746, 2020.
- J. Huang and R. Porter. Water wave propagation through arrays of closely spaced surface-piercing vertical barriers. *J. Fluid Mech.*, 960:A20, 2023.
- J. Li, A. L. Kohout, M. J. Doble, P. Wadhams, C. Guan, and H. H. Shen. Rollover of apparent wave attenuation in ice covered seas. *J. Geophys. Res.: Oceans*, 122:8557–8566, 2018.
- C. M. Linton. Water waves over arrays of horizontal cylinders: band gaps and bragg resonance. *J. Fluid Mech.*, 670:504–526, 2011.
- C. C. Mei, M. Stiassnie, and D. K. P. Yu. *Theory and application of ocean surface waves: Part I*. Wiley Interscience, New York, 2005.
- M. H. Meylan, L. G. Bennetts, and A. L. Kohout. In situ measurements and analysis of ocean waves in the antarctic marginal ice zone. *Geophys. Res. Lett.*, 41(14):5046–5051, 2014.
- M. H. Meylan, L. J. Yiew, L. G. Bennetts, B. J. French, and G. A. Thomas. Surge motion of an ice floe in waves: comparison of a theoretical and an experimental model. *Ann. Glaciol.*, 56(69):155–159, 2015.
- M. H. Meylan, L. G. Bennetts, J. E. M. Mosig, W. E. Rogers, M. J. Doble, and M. A. Peter. Dispersion relations, power laws, and energy loss for waves in the marginal ice zone. *J. Geophys. Res.: Oceans*, 123:3322–3335, 2018.
- J. E. M. Mosig, F. Montiel, and V. A. Squire. Water wave scattering from a mass loading ice floe of random length using generalised polynomial chaos. *Wave Motion*, 70:222–239, 2017.
- J. N. Newman. *Marine Hydrodynamics*. MIT Press, Cambridge, MA, 1977.
- J. P. A. Pitt and L. G. Bennetts. Model study of ocean wave propagation through broken sea ice covers with variable ice concentration. *Wave Motion*, 141:103655, 2026.

- W. E. Rogers, J. Thomson, H. H. Shen, M. J. Doble, P. Wadhams, and S. Cheng. Dissipation of wind waves by pancake and frazil ice in the autumn beaufort sea. *J. Geophys. Res.: Oceans*, 121(11):7991–8007, 2016.
- H. H. Shen and S. F. Ackley. A one-dimensional model for wave-induced ice-floe collisions. *Ann. Glaciol.*, 15:87–95, 1991.
- V. A. Squire. A fresh look at how ocean waves and sea ice interact. *Phil. Trans. Roy. Soc. A.*, 376:20170342, 2018.
- V. A. Squire. Ocean wave interactions with sea ice: A reappraisal. *Ann. Rev. Fluid Mech.*, 52(1):37–60, 2025.
- J. Thomson, L. Hošeková, M. H. Meylan, A. L. Kohout, and N. Kumar. Spurious rollover of wave attenuation rates in sea ice caused by noise in field measurements. *J. Geophys. Res.: Oceans*, 126(3):e2020JC016606, 2021.
- P. Wadhams, V. A. Squire, D. J. Goodman, A. M. Cowan, and S. C. Moore. The attenuation rates of ocean waves in the marginal ice zone. *J. Geophys. Res.*, 93(C6):6799–6818, 1988.
- M. Weitz and J. B. Keller. Reflection of water waves from floating ice in water of finite depth. *Comm. Pure & Appl. Math.*, 3(3):305–318, 1950.

WAVE PROPAGATION THROUGH PERIODIC ARRAYS OF FREELY FLOATING RECTANGULAR FLOES: SUPPLEMENTARY MATERIAL.

A PREPRINT

Lloyd Dafydd & Richard Porter

March 17, 2026

ABSTRACT

Using the definitions and notation introduced in the journal submission, we outline details of the calculations carried out for surge and pitch motions and the associated hydrodynamic forces that depend on these motions.

1 Solution in surge

A general expression for $\phi^{(s)}(x, y)$ in the fluid region $V^+ := \{0 < x < \ell, -\hat{\rho}d < z < 0\}$ satisfying both (2.1) and (2.12) is given by

$$\phi^{(s)}(x, z) = \varphi^{(s)}(x, z) + \sum_{m=0}^{\infty} a_m Z_m(z) \cos \alpha_m x \quad (\text{S.1.1})$$

where $\alpha_m = m\pi/\ell$ and

$$Z_0(z) = 1 + Kz, \quad Z_m(z) = \cosh \alpha_m z + (K/\alpha_m) \sinh \alpha_m z \quad (\text{S.1.2})$$

are chosen to satisfy (2.2). In (S.1.1), we have defined the particular solution satisfying (2.1), (2.2) and (2.11) and the boundary condition $\varphi_z^{(s)}(x, -\hat{\rho}d) = 0$

$$\begin{aligned} \varphi^{(s)}(x, z) = & \frac{1}{2\ell} \left(x^2 - (\ell - x)^2 e^{-ikL} \right) - \frac{1}{2\ell} \left(1 - e^{-ikL} \right) \left(z^2 + 2\hat{\rho}dz \right) \\ & - \left(\frac{\hat{\rho}d}{K\ell} + \frac{\ell}{6} \right) \left(1 - e^{-ikL} \right) + \sum_{m=1}^{\infty} \frac{2K \left((-1)^m - e^{-ikL} \right) \cos(\alpha_m x) \cosh[\alpha_m(z + \hat{\rho}d)]}{\ell \alpha_m^2 (\alpha_m \sinh(\alpha_m \hat{\rho}d) - K \cosh(\alpha_m \hat{\rho}d))}. \end{aligned} \quad (\text{S.1.3})$$

Over $0 < x < \ell$ we let $W^{(s)}(x) = \phi_z^{(s)}(x, -\hat{\rho}d)$ to represent the unknown vertical component of the fluid velocity across the interface between the two rectangular fluid sub-domains V^+ and V^- , above and below the level $z = -\hat{\rho}d$.

Using the orthogonality of the functions $\cos \alpha_m x$ (see (3.3)) then gives

$$(K \cosh(\alpha_m \hat{\rho}d) - \alpha_m \sinh(\alpha_m \hat{\rho}d)) a_m = \frac{2}{\ell} \int_0^{\ell} W^{(s)}(x) \cos \alpha_m x \, dx \quad (\text{S.1.4})$$

for $m = 0, 1, \dots$

In $z < -\hat{\rho}d$, the general solution satisfying (2.1), (2.4) and (2.11) can be written

$$\phi^{(s)}(x, z) = \sum_{m=-\infty}^{\infty} b_m e^{i\beta_m x} e^{\beta_m(z + \hat{\rho}d)} \quad (\text{S.1.5})$$

where $\beta_m = k + 2\pi m/L$. Using (3.7) now gives us

$$b_m = \frac{1}{\beta_m L} \int_0^{\ell} W^{(s)}(x) e^{-i\beta_m x} \, dx \quad (\text{S.1.6})$$

for all m . To complete the solution we match $\phi^{(s)}$ from (S.1.1) and (S.1.5) across $z = -\hat{\rho}d$, $0 < x < \ell$ and substitute expressions for a_m and b_m from (S.1.3), (S.1.6), a process which results in the integral equation

$$(\mathcal{T}W^{(s)})(x) \equiv \frac{1}{\ell} \int_0^\ell W^{(s)}(x')T(x, x') dx' = G^{(s)}(x), \quad 0 < x < \ell \quad (\text{S.1.7})$$

for the unknown function $W^{(s)}(x)$ where $T(x, x')$ is defined by (3.18) and we have defined

$$\begin{aligned} G^{(s)}(x) = (1/\ell)\varphi^{(s)}(x, -\hat{\rho}d) &= \frac{x^2}{2\ell^2} - \frac{(\ell-x)^2}{2\ell^2}e^{-ikL} + \left(\frac{d^2}{\ell^2} \left(\frac{\hat{\rho}^2}{2} - \frac{\hat{\rho}}{Kd} \right) - \frac{1}{6} \right) (1 - e^{-ikL}) \\ &\quad - \frac{2}{\ell^2} \sum_{m=1}^{\infty} \frac{((-1)^m - e^{-ikL}) \cos \alpha_m x}{\alpha_m^2 (\cosh(\alpha_m \hat{\rho}d) - (\alpha_m/K) \sinh(\alpha_m \hat{\rho}d))} \end{aligned} \quad (\text{S.1.8})$$

which has been determined from (S.1.3).

In order to use the solution $W^{(s)}(x)$ of (S.1.7) to calculate the surge-induced surge force $F^{(s,s)}$ directly, we use Green's identity with the functions $\phi^{(s)}(x, z)$ and $\overline{\varphi^{(s)}}(x, z)$ in the region V^+ and this gives us

$$\begin{aligned} 0 &= \int_{\partial V^+} \frac{\partial \phi^{(s)}}{\partial n} \overline{\varphi^{(s)}} - \frac{\partial \overline{\varphi^{(s)}}}{\partial n} \phi^{(s)} ds \\ &= - \int_0^\ell \left(\frac{\partial \phi^{(s)}}{\partial z} \overline{\varphi^{(s)}} - \frac{\partial \overline{\varphi^{(s)}}}{\partial z} \phi^{(s)} \right) \Big|_{z=-\hat{\rho}d} dx + \int_0^\ell \left(\frac{\partial \phi^{(s)}}{\partial z} \overline{\varphi^{(s)}} - \frac{\partial \overline{\varphi^{(s)}}}{\partial z} \phi^{(s)} \right) \Big|_{z=0} dx \\ &\quad + \int_{-\hat{\rho}d}^0 \left(\frac{\partial \phi^{(s)}}{\partial x} \overline{\varphi^{(s)}} - \frac{\partial \overline{\varphi^{(s)}}}{\partial x} \phi^{(s)} \right) \Big|_{x=\ell} dz - \int_{-\hat{\rho}d}^0 \left(\frac{\partial \phi^{(s)}}{\partial x} \overline{\varphi^{(s)}} - \frac{\partial \overline{\varphi^{(s)}}}{\partial x} \phi^{(s)} \right) \Big|_{x=0} dz \\ &= - \int_0^\ell W^{(s)}(x) \overline{\varphi^{(s)}}(x, -\hat{\rho}d) dx + \int_{-\hat{\rho}d}^0 \overline{\varphi^{(s)}}(\ell, z) - \phi^{(s)}(\ell, z) dz - \int_{-\hat{\rho}d}^0 \overline{\varphi^{(s)}}(0, z) e^{-ikL} - \phi^{(s)}(0, z) e^{ikL} dz \end{aligned} \quad (\text{S.1.9})$$

using the conditions satisfied by the two functions on the four boundaries and rearranging gives

$$\int_{-\hat{\rho}d}^0 \phi^{(s)}(\ell, z) - e^{ikL} \phi^{(s)}(0, z) dz = \int_{-\hat{\rho}d}^0 \overline{\varphi^{(s)}}(\ell, z) - \overline{\varphi^{(s)}}(0, z) e^{-ikL} dz - \int_0^\ell W^{(s)}(x) \overline{\varphi^{(s)}}(x, -\hat{\rho}d) dx. \quad (\text{S.1.10})$$

From the definition (2.13) we have

$$\begin{aligned} F^{(s,s)} &= \frac{1}{d(L-\ell)} \int_{-\hat{\rho}d}^0 \phi^{(s)}(\ell, z) - \phi^{(s)}(0, z) e^{ikL} dz \\ &= -\frac{\ell^2}{d(L-\ell)} A^{(s,s)} + C^{(s,s)} \end{aligned} \quad (\text{S.1.11})$$

after substituting from (S.1.10) and using the definition (S.1.7). For convenience we have defined

$$A^{(s,s)} = \frac{1}{\ell} \int_0^\ell W^{(s)}(x) \overline{G^{(s)}}(x) dx \quad (\text{S.1.12})$$

and

$$C^{(s,s)} = \frac{1}{d(L-\ell)} \int_{-\hat{\rho}d}^0 \overline{\varphi^{(s)}}(\ell, z) - \overline{\varphi^{(s)}}(0, z) e^{-ikL} dz \quad (\text{S.1.13})$$

in the above. Using the definition (S.1.3), we can calculate

$$C^{(s,s)} = \frac{\ell \hat{\rho}}{L-\ell} - \frac{4\hat{\rho}d^2 \sin^2(kL/2)}{\ell(L-\ell)} \left(\frac{\ell^2}{6d^2} + \frac{\hat{\rho}}{Kd} - \frac{\hat{\rho}^2}{3} \right) + \frac{4}{\ell(L-\ell)d} \sum_{m=1}^{\infty} \frac{(1 - (-1)^m \cos kL)}{\alpha_m^3 ((\alpha_m/K) - \coth(\alpha_m \hat{\rho}d))}. \quad (\text{S.1.14})$$

1.1 Numerical approximation

Following the example of heave in the main paper, we write

$$W^{(s)}(x) \approx \sum_{n=0}^N A_n^{(s)} u_n(x) \quad (\text{S.1.15})$$

for unknowns $A_n^{(s)}$ and with $u_n(x)$ defined by (3.30). After substituting into (S.1.7), multiplying by $\overline{u_m(x)}$ and integrating over $0 < x < \ell$ one obtains

$$\sum_{n=0}^N A_n^{(s)} T_{mn} = E_m^{(s)} \quad (\text{S.1.16})$$

where T_{mn} is given by (3.28) whilst

$$E_m^{(s)} = \int_0^\ell G^{(s)}(x) \overline{u_m(x)} dx. \quad (\text{S.1.17})$$

From the definition (S.1.3) we find

$$E_m^{(s)} = \mathcal{K}_m + \left(-\frac{\hat{\rho}^2 d^2}{2\ell^2} + \frac{\hat{\rho} d}{K\ell^2} + \frac{1}{6} \right) (1 - e^{-ikL}) \overline{I_{m0}} + \sum_{n=1}^{\infty} \frac{2K((-1)^n - e^{-ikL}) \overline{I_{mn}}}{\alpha_n^2 \ell^2 (\alpha_n \sinh(\alpha_n \hat{\rho} d) - K \cosh(\alpha_n \hat{\rho} d))}, \quad (\text{S.1.18})$$

where I_{mn} is defined by (3.31), (3.32) and we have had to make a new calculation $\mathcal{K}_m = \langle g, u_m \rangle$ where $g(x) = (x^2 - (\ell - x)^2 e^{-ikL}) / (2\ell^2)$ and find, using some standard integral results for products of polynomials and Gegenbauer polynomials (REF), that

$$\mathcal{K}_m = \frac{i^m 2^{1/6} \Gamma(8/3)}{\sqrt{\pi} \Gamma(m + 10/3) \Gamma(3 - m)} ((-1)^m - e^{-ikL}) \quad (\text{S.1.19})$$

noting that, for $m \geq 3$, we have $\mathcal{K}_m = 0$.

Finally, it follows from using (S.1.15) in (S.1.12) that

$$A^{(s,s)} \approx \sum_{n=0}^N A_n^{(s)} \overline{E_n^{(s)}}. \quad (\text{S.1.20})$$

1.2 Asymptotic results for small gaps

Letting $\ell/d = \epsilon \ll 1$ and assuming $|K\hat{\rho}d - 1| \gg \epsilon$ (away from resonance) we have as before, from (3.40),

$$T(x, x') \approx \epsilon^{-1} \tilde{T}, \quad \text{where } \tilde{T} = \frac{K\hat{\rho}d - 1}{Kd} + \frac{1}{2} \epsilon \cot\left(\frac{kL}{2}\right). \quad (\text{S.1.21})$$

We also have from (S.1.8) the leading order behaviour

$$G^{(s)}(x) \approx \frac{1}{\epsilon^2} \tilde{G}^{(s)}, \quad \text{where } \tilde{G}^{(s)} = \left(\frac{\hat{\rho}^2}{2} - \frac{\hat{\rho}}{Kd} \right) (1 - e^{-ikL}). \quad (\text{S.1.22})$$

Using (S.1.21) and (S.1.22) in (S.1.7) gives

$$\frac{1}{\ell} \int_0^\ell W^{(s)}(x') dx' \approx \frac{1}{\epsilon} \frac{\tilde{G}^{(s)}}{\tilde{T}} \quad (\text{S.1.23})$$

which when used in (S.1.13) gives

$$A^{(s,s)} \approx \frac{1}{\epsilon^3} \frac{|\tilde{G}^{(s)}|^2}{\tilde{T}}. \quad (\text{S.1.24})$$

Also, the leading order behaviour in (S.1.14) gives

$$C^{(s,s)} \approx \frac{1}{\epsilon} \frac{4\hat{\rho}^2}{KL} \left(\frac{1}{3} K\hat{\rho}d - 1 \right) \sin^2\left(\frac{kL}{2}\right). \quad (\text{S.1.25})$$

Using (S.1.24) and (S.1.25) with (S.1.21) and (S.1.22) in (S.1.11) and simplifying shows us that

$$F^{(s,s)} \approx \frac{1}{\epsilon} \frac{4\hat{\rho}^2 d}{KL} \sin^2\left(\frac{kL}{2}\right) \left(\frac{1}{3} K\hat{\rho}d - 1 - \frac{(K\hat{\rho}d - 2)^2}{4(K\hat{\rho}d - 1) + 2\epsilon Kd \cot(kL/2)} \right) \quad (\text{S.1.26})$$

is the leading order behaviour of the surge-induced surge force for $\epsilon \ll 1$ away from resonance.

2 Combined heave-surge forces

We are now in a position to consider the heave-induced surge force and the surge-induced heave force (theory dictates that are complex conjugates).

We see from the definition (2.13) that

$$F^{(h,s)} = \frac{1}{d(L-\ell)} \int_{-\hat{\rho}d}^0 \phi^{(h)}(\ell, z) dz - \frac{e^{ikL}}{d(L-\ell)} \int_{-\hat{\rho}d}^0 \phi^{(h)}(0, z) dz \quad (\text{S.2.1})$$

and

$$F^{(s,h)} = \frac{1}{d(L-\ell)} \int_{\ell}^L \phi^{(s)}(x, -\hat{\rho}d) dx. \quad (\text{S.2.2})$$

Applying Green's identity to $\phi^{(h)}(x, z)$ and $\overline{\varphi^{(s)}}(x, z)$ in the region V^+ we get, using all of the equations and boundary conditions defining those functions

$$\int_{-\hat{\rho}d}^0 \phi^{(h)}(\ell, z) dz - e^{ikL} \int_{-\hat{\rho}d}^0 \phi^{(h)}(0, z) dz = -\ell \int_0^{\ell} W^{(h)}(x) \overline{G^{(s)}(x)} dx. \quad (\text{S.2.3})$$

Instead, applying Green's identity to $\phi^{(s)}(x, z)$ and $\overline{\varphi^{(h)}}(x, z)$ in the region V^- and again using all of the equations and boundary conditions defining those functions

$$\int_{\ell}^L \phi^{(s)}(x, -\hat{\rho}d) dx = -\ell \int_0^{\ell} W^{(s)}(x) \overline{G^{(h)}(x)} dx. \quad (\text{S.2.4})$$

Combining (S.2.3), (S.2.4) with (S.2.1), (S.2.2) results in

$$F^{(h,s)} = -\frac{\ell^2}{d(L-\ell)} A^{(h,s)}, \quad \text{where } A^{(h,s)} = \frac{1}{\ell} \int_0^{\ell} W^{(h)}(x) \overline{G^{(s)}(x)} dx \quad (\text{S.2.5})$$

and

$$F^{(s,h)} = -\frac{\ell^2}{d(L-\ell)} A^{(s,h)}, \quad \text{where } A^{(s,h)} = \int_0^{\ell} W^{(s)}(x) \overline{G^{(h)}(x)} dx. \quad (\text{S.2.6})$$

2.1 Numerical approximation

The numerical approximations to these quantities above are obtained from

$$A^{(h,s)} \approx \sum_{n=0}^N A_n^{(h)} \overline{E_n^{(s)}} \quad (\text{S.2.7})$$

and

$$A^{(s,h)} \approx \sum_{n=0}^N A_n^{(s)} \overline{E_n^{(h)}}. \quad (\text{S.2.8})$$

Use of the integral equations, $(\mathcal{T}W^{(s,h)})(x) = G^{(s,h)}(x)$, satisfied by $W^{(s,h)}(x)$ gives

$$A^{(h,s)} = \langle W^{(h)}, G^{(s)} \rangle = \langle W^{(h)}, \mathcal{T}W^{(s)} \rangle = \langle \mathcal{T}W^{(h)}, W^{(s)} \rangle = \langle G^{(h)}, W^{(s)} \rangle = \overline{A^{(s,h)}}. \quad (\text{S.2.9})$$

This means $F^{(h,s)} = \overline{F^{(s,h)}}$ confirming the identity (2.17) in the main paper and thus we only need consider $F^{(h,s)}$.

2.2 Asymptotic analysis for small gaps

Using (3.37), (S.1.21) and (S.1.22) we can immediately write

$$A^{(h,s)} \approx \frac{1}{\epsilon^2} \frac{\tilde{G}^{(h)} \overline{\tilde{G}^{(s)}}}{\tilde{T}}, \quad \text{and} \quad A^{(s,h)} \approx \frac{1}{\epsilon^2} \frac{\tilde{G}^{(s)} \overline{\tilde{G}^{(h)}}}{\tilde{T}} \quad (\text{S.2.10})$$

and so, by (S.2.5), (S.2.6) the leading order approximation of the surge/heave forces for small gaps are defined by the expression

$$F^{(h,s)} = i\hat{\rho} \frac{\frac{1}{2}K\hat{\rho}d - 1}{K\hat{\rho}d - 1 + \frac{1}{2}\epsilon Kd \cot\left(\frac{kL}{2}\right)}. \quad (\text{S.2.11})$$

3 Solution in Pitch

This is the most complicated problem to solve because the forcing applies on all sides of the submerged rectangular floe and so particular solutions are required in both V^+ and V^- .

A general expression for the potential $\phi^{(p)}(x, z)$ in the fluid region $V^+ := \{0 < x < \ell, -\hat{\rho}d < z < 0\}$ satisfying (2.1), (2.2) and (2.12) can be written as

$$\phi^{(p)}(x, z) = \varphi^{(+p)}(x, z) + \sum_{m=0}^{\infty} a_m Z_m(z) \cos \alpha_m x \quad (\text{S.3.1})$$

where $\alpha_m = m\pi/\ell$ and

$$Z_0(z) = 1 + Kz, \quad Z_m(z) = \cosh \alpha_m z + (K/\alpha_m) \sinh \alpha_m z \quad (\text{S.3.2})$$

are defined as before. The function $\varphi^{(+p)}(x, z)$ satisfies (2.1), (2.2) and the inhomogeneous condition (2.11) as well as the imposed condition $\psi_z^{(+p)}(x, -\hat{\rho}d) = 0$. After considerable effort, we find it can be written

$$\begin{aligned} \varphi^{(+p)}(x, z) &= \frac{1}{2\ell} \left(x^2 - (\ell - x)^2 e^{-ikL} \right) \frac{(z - z^c)}{L - \ell} - \frac{1}{6\ell} \left(1 - e^{-ikL} \right) \frac{((z - z^c)^3 - 3(z^c + \hat{\rho}d)^2 z + \ell^2(z - z^c))}{L - \ell} \\ &\quad + \frac{(3\hat{\rho}d(2z^c + \hat{\rho}d) - Kz^c)}{6K(L - \ell)\ell} \left(1 - e^{-ikL} \right) \\ &\quad - \frac{2}{\ell(L - \ell)} \sum_{m=1}^{\infty} \frac{((-1)^m - e^{-ikL})}{\alpha_m^3 \cosh(\alpha_m \hat{\rho}d)} \cos(\alpha_m x) (\sinh[\alpha_m z] + C_m \cosh[\alpha_m(z + \hat{\rho}d)]) \end{aligned} \quad (\text{S.3.3})$$

where

$$C_m = \frac{\alpha_m (\text{sech}(\alpha_m \hat{\rho}d) - 1 - Kz^c)}{K - \alpha_m \tanh(\alpha_m \hat{\rho}d)}. \quad (\text{S.3.4})$$

We are reminded that $z^c = (\frac{1}{2} - \hat{\rho})d$ is the z coordinate of the centre of mass. In deriving this expression we have, in turn, satisfied the inhomogeneous boundary conditions (2.11) on $x = 0$, $x = \ell$, and then Laplace's equation, followed by the condition on $z = -\hat{\rho}d$ and finally the condition on $z = 0$.

After taking the z -derivative of (S.3.1), evaluated on $z = -\hat{\rho}d$, multiplying by $\cos \alpha_m x$ and integrating over $0 < x < \ell$ we find, for $m = 0$,

$$a_0 = \frac{1}{K\ell} \int_0^\ell W^{(p)}(x) dx \quad (\text{S.3.5})$$

where we have let $W^{(p)}(x) = \phi_z^{(p)}(x, -\hat{\rho}d)$ for $0 < x < \ell$. For $m \geq 1$,

$$(K \cosh(\alpha_m \hat{\rho}d) - \alpha_m \sinh(\alpha_m \hat{\rho}d)) a_m = \frac{2}{\ell} \int_0^\ell W^{(p)}(x) \cos \alpha_m x dx. \quad (\text{S.3.6})$$

In $z < -\hat{\rho}d$, we require a general solution to satisfy (2.1), (2.4) and (2.11) and thus write

$$\phi^{(p)}(x, z) = \varphi^{(-p)}(x, z) + \sum_{m=-\infty}^{\infty} b_m e^{i\beta_m x} e^{\beta_m(z + \hat{\rho}d)} \quad (\text{S.3.7})$$

where $\beta_m = k + 2\pi m/L$ as before. Here, we have defined $\varphi^{(-p)}(x, z)$ to be the harmonic function satisfying (2.4) and decaying into the depth in addition to the imposed condition

$$\varphi_z^{(-p)}(x, -\hat{\rho}d) = \begin{cases} -(x - x^c)/(L - \ell), & \ell < x < L \\ 0, & 0 < x < \ell \end{cases} \quad (\text{S.3.8})$$

which accounts for the forcing on the underside of the floe in much the same way as $\varphi^{(+p)}(x, z)$ accounted for the forcing on the sides of the floe in V^+ .

The particular solution can be determined by writing the separation series satisfying (2.1) and (2.4)

$$\varphi^{(-p)}(x, z) = \ell \sum_{m=-\infty}^{\infty} \frac{g_m^{(p)} e^{i\beta_m x}}{\beta_m L} e^{\beta_m(z + \hat{\rho}d)} \quad (\text{S.3.9})$$

where (S.3.8) tells us that

$$\ell g_m^{(p)} = -\frac{1}{(L-\ell)} \int_{\ell}^L (x-x^c) e^{-i\beta_m x} dx = \frac{e^{-i\beta_m \ell} - e^{-i\beta_m L}}{\beta_m^2 (L-\ell)} + \frac{1}{2} \frac{e^{-i\beta_m \ell} + e^{-i\beta_m L}}{i\beta_m} \quad (\text{S.3.10})$$

after using the orthogonality of the functions $e^{i\beta_m x}$ on $0 < x < L$ expressed by (3.10). As a result of taking the z -derivative of (S.3.7) on $z = -\hat{\rho}d$, we find

$$b_m = \frac{1}{\beta_m L} \int_0^{\ell} W^{(p)}(x) e^{-i\beta_m x} dx \quad (\text{S.3.11})$$

for all m . Next, applying continuity of $\phi^{(p)}$ across the common interface $z = -\hat{\rho}d$, $0 < x < \ell$ between the two regions and substituting for a_m and b_m from (S.3.6), (S.3.11) results in the integral equation

$$(\mathcal{T}W^{(p)})(x) \equiv \frac{1}{\ell} \int_0^{\ell} W^{(p)}(x') T(x, x') dx' = G^{(p)}(x), \quad 0 < x < \ell \quad (\text{S.3.12})$$

where $T(x, x')$ is defined by (3.18) and we have defined the function

$$G^{(p)}(x) = (1/\ell) \left(\varphi^{(+p)}(x, -\hat{\rho}d) - \varphi^{(-p)}(x, -\hat{\rho}d) \right). \quad (\text{S.3.13})$$

Using Green's identity with the functions two harmonic functions $\phi^{(p)}(x, z)$ and $\overline{\varphi^{(-p)}}(x, z)$ in the region V^- and using all of the conditions of these functions on the boundary of V^- gives us

$$\begin{aligned} 0 &= \int_{V^-} \frac{\partial \phi^{(p)}}{\partial n} \overline{\varphi^{(-p)}} - \frac{\partial \overline{\varphi^{(-p)}}}{\partial n} \phi^{(p)} ds \\ &= \int_0^{\ell} \left(\frac{\partial \phi^{(p)}}{\partial z} \overline{\varphi^{(-p)}} - \frac{\partial \overline{\varphi^{(-p)}}}{\partial z} \phi^{(p)} \right) \Big|_{z=-\hat{\rho}d} dx + \int_{\ell}^L \left(\frac{\partial \phi^{(p)}}{\partial z} \overline{\varphi^{(-p)}} - \frac{\partial \overline{\varphi^{(-p)}}}{\partial z} \phi^{(p)} \right) \Big|_{z=-\hat{\rho}d} dx \\ &= \int_0^{\ell} W^{(h)}(x) \overline{\varphi^{(-p)}}(x, -\hat{\rho}d) dx - \int_{\ell}^L \frac{x-x^c}{L-\ell} \left(\overline{\varphi^{(-p)}}(x, -\hat{\rho}d) - \phi(x, -\hat{\rho}d) \right) dx \end{aligned} \quad (\text{S.3.14})$$

from which we can clearly see

$$\int_{\ell}^L \frac{x-x^c}{L-\ell} \phi^{(p)}(x, -\hat{\rho}d) dx = - \int_0^{\ell} W^{(p)}(x) \overline{\varphi^{(-p)}}(x, -\hat{\rho}d) dx + \int_{\ell}^L \frac{x-x^c}{L-\ell} \overline{\varphi^{(-p)}}(x, -\hat{\rho}d) dx. \quad (\text{S.3.15})$$

Separately we use Green's identity with $\phi^{(p)}(x, z)$ and $\overline{\varphi^{(+p)}}(x, z)$ in V^+ which results, after some algebra, in the relation

$$\begin{aligned} \int_{-\hat{\rho}d}^0 \frac{z-z^c}{L-\ell} \left(\phi^{(p)}(\ell, z) - e^{ikL} \phi^{(p)}(0, z) \right) dz &= - \int_0^{\ell} W^{(p)}(x) \overline{\varphi^{(+p)}}(x, -\hat{\rho}d) dx \\ &+ \int_{-\hat{\rho}d}^0 \frac{z-z^c}{L-\ell} \left(\overline{\varphi^{(+p)}}(\ell, z) - \overline{\varphi^{(+p)}}(0, z) e^{-ikL} \right) dz \end{aligned} \quad (\text{S.3.16})$$

Now, from the general formula (2.13) we can deduce that the pitch-induced pitch force is expressed in terms of the potential $\phi^{(p)}$ as

$$F^{(p,p)} = -\frac{1}{d(L-\ell)^2} \int_{\ell}^L \phi^{(p)}(x, -\hat{\rho}d) (x-x^c) dx + \frac{1}{d(L-\ell)^2} \int_{-\hat{\rho}d}^0 (z-z^c) \left(\phi^{(p)}(\ell, z) - \phi^{(p)}(0, z) e^{ikL} \right) dz. \quad (\text{S.3.17})$$

Using (S.3.15) and (S.3.16) in (S.3.17) along with the definition (S.3.13) gives

$$\begin{aligned} F^{(p,p)} &= -\frac{\ell}{d(L-\ell)} \int_0^{\ell} W^{(p)}(x) \overline{G^{(p)}}(x) dx - \frac{1}{d(L-\ell)^2} \int_{\ell}^L (x-x^c) \overline{\varphi^{(-p)}}(x, -\hat{\rho}d) dx \\ &+ \frac{1}{d(L-\ell)^2} \int_{-\hat{\rho}d}^0 (z-z^c) \left(\overline{\varphi^{(+p)}}(\ell, z) - \overline{\varphi^{(+p)}}(0, z) e^{-ikL} \right) dz. \end{aligned} \quad (\text{S.3.18})$$

Thus, we have written $F^{(p,p)}$ in terms of the solution, $W^{(p)}(x)$, of (S.3.12) plus integrals of known functions. It helps to write

$$F^{(p,p)} = -\frac{\ell^2}{d(L-\ell)} A^{(p,p)} + C^{(p,p)} \quad (\text{S.3.19})$$

where

$$A^{(p,p)} = \frac{1}{\ell} \int_0^\ell W^{(p)}(x) \overline{G^{(p)}(x)} dx \quad (\text{S.3.20})$$

and

$$C^{(p,p)} = C_1^{(p,p)} + C_2^{(p,p)} \quad (\text{S.3.21})$$

with: (i)

$$C_1^{(p,p)} = -\frac{1}{d(L-\ell)^2} \int_\ell^L (x-x^c) \overline{\varphi^{(-p)}(x, -\hat{\rho}d)} dx = \frac{\ell^2}{d(L-\ell)} \sum_{m=-\infty}^{\infty} \frac{|g_m^{(p)}|^2}{\beta_m L} = 0 \quad (\text{S.3.22})$$

a result which is proved in the Appendix; and (ii)

$$C_2^{(p,p)} = \frac{1}{d(L-\ell)^2} \int_{-\hat{\rho}d}^0 (z-z^c) \left(\overline{\varphi^{(+p)}(\ell, z)} - \overline{\varphi^{(+p)}(0, z)} e^{-ikL} \right) dz. \quad (\text{S.3.23})$$

A considerable amount of algebra allows us to determine

$$\begin{aligned} C^{(p,p)} &= \frac{\ell d^2 \hat{\rho}}{(L-\ell)^3} \left(\frac{\hat{\rho}^2}{3} - \frac{\hat{\rho}}{2} + \frac{1}{4} \right) + \frac{d^4 \sin^2(kL/2)}{\ell(L-\ell)^3} \left(\frac{\hat{\rho}^5}{5} - \frac{\hat{\rho}^4}{2} + \frac{\hat{\rho}^3}{3} - \frac{\hat{\rho}^2(1-\hat{\rho})^2}{Kd} - \frac{\ell^2}{d^2} \left(\frac{2\hat{\rho}^3}{9} - \frac{\hat{\rho}^2}{3} + \frac{\hat{\rho}}{6} \right) \right) \\ &\quad - \frac{4}{d\ell(L-\ell)^3} \sum_{m=1}^{\infty} \frac{(1-(-1)^m \cos(kL))}{\alpha_m^5 \cosh(\alpha_m \hat{\rho}d)} \left(\alpha_n \hat{\rho}d - (1 + \frac{1}{2} C_m \alpha_m d)(1 - e^{-\alpha_m \hat{\rho}d}) \right). \end{aligned} \quad (\text{S.3.24})$$

3.1 Numerical approximation

We follow the same methods as before, and start by writing

$$W^{(p)}(x) \approx \sum_{n=0}^N A_n^{(p)} u_n(x) \quad (\text{S.3.25})$$

which, when used in (S.3.11) under Galerkin's method, results in the expansion coefficients $A_n^{(p)}$ being determined by the linear system of equations

$$\sum_{n=0}^N A_n^{(p)} T_{mn} = E_m^{(p)}, \quad (\text{S.3.26})$$

where

$$E_m^{(p)} = \frac{1}{\ell} \int_0^\ell G^{(p)}(x) \overline{u_m(x)} dx. \quad (\text{S.3.27})$$

Using the definitions of $G^{(p)}(x)$ and $u_m(x)$ from (S.3.13) and ((3.35)) we find, again after considerable algebra,

$$\begin{aligned} E_m^{(p)} &= -\sum_{n=-\infty}^{\infty} \frac{g_n^{(p)}}{\beta_n L} \overline{\mathcal{J}_{mn}} - \frac{d}{2(L-\ell)} \mathcal{K}_m + \frac{d^3(1-e^{-ikL})}{6\ell^2(L-\ell)} \left(\frac{3\hat{\rho}(1-\hat{\rho})}{Kd} - \frac{\ell^2}{2d^2} + \hat{\rho}^3 - \frac{3\hat{\rho}^2}{2} \right) \overline{\mathcal{I}_{m0}} \\ &\quad - \frac{2}{\ell^2(L-\ell)} \sum_{n=1}^{\infty} \frac{((-1)^n - e^{-ikL})}{\alpha_n^3 \cosh(\alpha_n \hat{\rho}d)} (C_n - \sinh(\alpha_n \hat{\rho}d)) \overline{\mathcal{I}_{mn}}. \end{aligned} \quad (\text{S.3.28})$$

In the above \mathcal{K}_m is defined by (S.1.19) and \mathcal{J}_{mn} and \mathcal{I}_{mn} are defined in the main paper.

Finally, from (S.3.26) in (S.3.28) we have

$$A^{(p,p)} \approx \sum_{n=0}^N A_n^{(p)} \overline{E_m^{(p)}}. \quad (\text{S.3.29})$$

3.2 Asymptotic results for small gaps

First we note from the definition (S.3.13) that we can write

$$G^{(p)} \approx \frac{1}{\epsilon^2} \tilde{G}^{(p)} \quad (\text{S.3.30})$$

to leading order where

$$\tilde{G}^{(p)} = \frac{\hat{\rho}d}{2L}(1 - e^{-ikL}) \left(\frac{\hat{\rho}^2}{3} - \frac{\hat{\rho}}{2} + \frac{(1-\hat{\rho})}{Kd} \right). \quad (\text{S.3.31})$$

Using $T(x, x') \approx \epsilon^{-1}\tilde{T}$ where \tilde{T} is given by (3.35), the solution of (S.3.12) is approximated by

$$\frac{1}{\ell} \int_0^\ell W^{(p)}(x') dx' \approx \frac{1}{\epsilon} \frac{\tilde{G}^{(p)}}{\tilde{T}}. \quad (\text{S.3.32})$$

It follows from (S.3.20) that

$$A^{(p,p)} \approx \frac{1}{\epsilon^3} \frac{|\tilde{G}^{(p)}|^2}{\tilde{T}}. \quad (\text{S.3.33})$$

Simultaneously, we can show that the leading order behaviour of $C^{(p,p)}$ defined in (S.3.24), is

$$C^{(p,p)} \approx \frac{1}{\epsilon} \frac{d^3}{L^3} \hat{\rho}^2 \sin^2(kL/2) \left(\frac{\hat{\rho}^3}{5} - \frac{\hat{\rho}^2}{2} + \frac{\hat{\rho}}{3} - \frac{(1-\hat{\rho})^2}{Kd} \right). \quad (\text{S.3.34})$$

Bringing both results together in (S.3.19) gives

$$F^{(p,p)} = \frac{1}{\epsilon} \hat{\rho}^2 \left(\frac{d}{L} \right)^3 \left(\frac{\hat{\rho}^3}{5} - \frac{\hat{\rho}^2}{2} + \frac{\hat{\rho}}{3} - \frac{(1-\hat{\rho})^2}{Kd} - \frac{\left(\frac{\hat{\rho}^2}{3} - \frac{\hat{\rho}}{2} + \frac{1-\hat{\rho}}{Kd} \right)^2}{\frac{K\hat{\rho}d-1}{Kd} + \frac{1}{2}\epsilon \cot\left(\frac{kL}{2}\right)} \right) \sin^2\left(\frac{kL}{2}\right) \quad (\text{S.3.35})$$

as the leading order approximation to the pitch-induced pitch force away from resonance.

4 Combined heave-pitch forces

From (2.13) we express the pitch-induced heave force as

$$F^{(p,h)} = \frac{1}{d(L-\ell)} \int_\ell^L \phi^{(p)}(x, -\hat{\rho}d) dx \quad (\text{S.4.1})$$

after using the conditions satisfied by the $\phi^{(h)}$ on $z = -\hat{\rho}d, x = 0, \ell$. In order to express this in terms of solutions to the integral equations formulated for each problem, we use $\phi^{(p)}$ and $\varphi^{(h)}$ over V^- in Green's identity to get

$$\begin{aligned} 0 &= \int_{\partial V^-} \frac{\partial \phi^{(p)}}{\partial n} \overline{\varphi^{(h)}} - \frac{\partial \overline{\varphi^{(h)}}}{\partial n} \phi^{(p)} ds \\ &= \int_0^\ell \left(\frac{\partial \phi^{(p)}}{\partial z} \overline{\varphi^{(h)}} - \frac{\partial \overline{\varphi^{(h)}}}{\partial z} \phi^{(p)} \right) \Big|_{z=-\hat{\rho}d} dx + \int_\ell^L \left(\frac{\partial \phi^{(p)}}{\partial z} \overline{\varphi^{(h)}} - \frac{\partial \overline{\varphi^{(h)}}}{\partial z} \phi^{(p)} \right) \Big|_{z=-\hat{\rho}d} dx \\ &= \int_0^\ell W^{(p)}(x) \overline{\varphi^{(h)}}(x, -\hat{\rho}d) dx - \int_\ell^L \frac{x-x^c}{L-\ell} \overline{\varphi^{(h)}}(x, -\hat{\rho}d) + \phi^{(p)}(x, -\hat{\rho}d) dx. \end{aligned} \quad (\text{S.4.2})$$

Therefore, we can write

$$F^{(p,h)} = -\frac{\ell^2}{d(L-\ell)} A^{(p,h)} + C^{(p,h)} \quad (\text{S.4.3})$$

where

$$A^{(p,h)} = \frac{1}{\ell} \int_0^\ell W^{(p)}(x) \overline{G^{(h)}}(x) dx \quad (\text{S.4.4})$$

with $G^{(h)}$ defined by (3.14) and

$$C^{(p,h)} = \frac{\ell}{d(L-\ell)} \int_\ell^L \frac{x-x^c}{L-\ell} \overline{G^{(h)}}(x) dx. \quad (\text{S.4.5})$$

Using the definition (3.14) with (S.3.10) allows us to write

$$C^{(p,h)} = \frac{\ell^2}{d(L-\ell)} \sum_{m=-\infty}^{\infty} \frac{\overline{g_m^{(h)}} g_m^{(p)}}{\beta_m L}. \quad (\text{S.4.6})$$

In Appendix A we show that

$$C^{(p,h)} = -i \frac{(L-\ell)}{12d}. \quad (\text{S.4.7})$$

We now consider the reciprocal heave-induced pitch force. From (2.13) we express the heave-induced pitch force as

$$F^{(h,p)} = -\frac{1}{d(L-\ell)^2} \int_{\ell}^L (x-x^c) \phi^{(h)}(x, -\hat{\rho}d) dx + \frac{1}{d(L-\ell)^2} \int_{-\hat{\rho}d}^0 (z-z^c) \left(\phi^{(h)}(\ell, z) - e^{ikL} \phi^{(h)}(0, z) \right) dz \quad (\text{S.4.8})$$

after using the conditions satisfied by the $\phi^{(p)}$ on $z = -\hat{\rho}d, x = 0, \ell$. Using $\phi^{(h)}$ and $\varphi^{(+p)}$ in Green's identity over the region V^+ we find

$$\begin{aligned} 0 &= \int_0^{\ell} \left(\frac{\partial \phi^{(h)}}{\partial z} \overline{\varphi^{(+p)}} - \frac{\partial \overline{\varphi^{(+p)}}}{\partial z} \phi^{(h)} \right) \Big|_{z=-\hat{\rho}d} dx - \int_0^{\ell} \left(\frac{\partial \phi^{(h)}}{\partial z} \overline{\varphi^{(+p)}} - \frac{\partial \overline{\varphi^{(+p)}}}{\partial z} \phi^{(h)} \right) \Big|_{z=0} dx \\ &+ \int_{-\hat{\rho}d}^0 \left(\frac{\partial \phi^{(h)}}{\partial x} \overline{\varphi^{(+p)}} - \frac{\partial \overline{\varphi^{(+p)}}}{\partial x} \phi^{(h)} \right) \Big|_{x=\ell} dz - \int_{-\hat{\rho}d}^0 \left(\frac{\partial \phi^{(h)}}{\partial x} \overline{\varphi^{(+p)}} - \frac{\partial \overline{\varphi^{(+p)}}}{\partial x} \phi^{(h)} \right) \Big|_{x=0} dz \\ &= - \int_0^{\ell} W^{(h)}(x) \overline{\varphi^{(+p)}}(x, -\hat{\rho}d) dx - \int_{-\hat{\rho}d}^0 \frac{(z-z^c)}{(L-\ell)} \left(\phi^{(h)}(\ell, z) - e^{ikL} \phi^{(h)}(0, z) \right) dz. \end{aligned} \quad (\text{S.4.9})$$

Also, using $\phi^{(h)}$ and $\varphi^{(-p)}$ in Green's identity in the domain V^- gives

$$\begin{aligned} 0 &= \int_0^L \left(\frac{\partial \phi^{(h)}}{\partial z} \overline{\varphi^{(-p)}} - \frac{\partial \overline{\varphi^{(-p)}}}{\partial z} \phi^{(h)} \right) \Big|_{z=-\hat{\rho}d} dx \\ &= \int_0^{\ell} W^{(h)}(x) \overline{\varphi^{(-p)}}(x, -\hat{\rho}d) dx + \int_{\ell}^L \overline{\varphi^{(-p)}}(x, -\hat{\rho}d) + \frac{(x-x^c)}{(L-\ell)} \phi^{(h)}(x, -\hat{\rho}d) dx. \end{aligned} \quad (\text{S.4.10})$$

Using both (S.4.9) and (S.4.10) in (S.4.8) along with (S.3.13) results in

$$F^{(h,p)} = -\frac{\ell^2}{d(L-\ell)} A^{(h,p)} + C^{(h,p)} \quad (\text{S.4.11})$$

where we have defined

$$A^{(h,p)} = \frac{1}{\ell} \int_0^{\ell} W^{(h)}(x) \overline{G^{(p)}}(x) dx \quad (\text{S.4.12})$$

and

$$C^{(h,p)} = \frac{1}{d(L-\ell)} \int_{\ell}^L \overline{\varphi^{(-p)}}(x, -\hat{\rho}d) dx = \frac{\ell^2}{d(L-\ell)} \sum_{m=-\infty}^{\infty} \frac{\overline{g_m^{(p)}} g_m^{(h)}}{\beta_m L} \quad (\text{S.4.13})$$

which follows from use of (3.8) and (S.3.9). Clearly $C^{(h,p)} = \overline{C^{(p,h)}}$ whilst $A^{(h,p)} = \overline{A^{(p,h)}}$ using the same reasoning outlined in the surge/heave section.

4.1 Numerical approximation

We simply have

$$\tilde{A}^{(h,p)} \approx \sum_{n=0}^N A_n^{(h)} \overline{E_n^{(p)}} \quad (\text{S.4.14})$$

and

$$\tilde{A}^{(p,h)} \approx \sum_{n=0}^N A_n^{(p)} \overline{E_n^{(h)}} \quad (\text{S.4.15})$$

where $A_n^{(h,p)}$ are the coefficients determined from (3.23) and (S.3.26) and $E_n^{(h,p)}$ are defined by (3.29) and (S.3.27) respectively.

4.2 Asymptotic results for small gaps

Using the leading order terms in the integral equations, we find

$$A^{(h,p)} \approx \frac{1}{\epsilon^2} \frac{\overline{\tilde{G}^{(p)}} \tilde{G}^{(h)}}{\tilde{T}}. \quad (\text{S.4.16})$$

Using (3.35), (3.37) and (S.3.31) and simplifying results whilst using $C^{(h,p)} = iL/12d$ from (S.4.7), we have from (S.4.11),

$$F^{(h,p)} = i \left(\frac{L}{12d} + \frac{\hat{\rho}d}{2L} \frac{\frac{\hat{\rho}^2}{3} - \frac{\hat{\rho}}{2} + \frac{1-\hat{\rho}}{Kd}}{\frac{K\hat{\rho}d-1}{Kd} + \frac{\epsilon}{2} \cot\left(\frac{kL}{2}\right)} \right) \quad (\text{S.4.17})$$

is the leading order heave-induced pitch force for small gaps. $F^{(p,h)}$ is the conjugate of (S.4.17)

5 Combined surge-pitch forces

Following the methodology used for the previous problems we are able to show that

$$F^{(s,p)} = -\frac{\ell^2}{d(L-\ell)} A^{(s,p)} + C^{(s,p)} \quad (\text{S.5.1})$$

where

$$A^{(s,p)} = \frac{1}{\ell} \int_0^\ell W^{(s)}(x) \overline{G^{(p)}}(x) dx \quad (\text{S.5.2})$$

and

$$C^{(s,p)} = \frac{1}{d(L-\ell)} \int_{-\hat{\rho}d}^0 \overline{\varphi^{(+p)}}(\ell, z) - e^{-ikL} \overline{\varphi^{(+p)}}(0, z) dz, \quad (\text{S.5.3})$$

Likewise, for the reciprocal force, we have

$$F^{(p,s)} = -\frac{\ell^2}{d(L-\ell)} A^{(p,s)} + C^{(p,s)} \quad (\text{S.5.4})$$

where

$$A^{(p,s)} = \frac{1}{\ell} \int_0^\ell W^{(p)}(x) \overline{G^{(s)}}(x) dx \quad (\text{S.5.5})$$

and

$$C^{(p,s)} = \frac{1}{d(L-\ell)^2} \int_{-\hat{\rho}d}^0 (z - z^c) \left(\overline{\varphi^{(s)}}(\ell, z) - e^{-ikL} \overline{\varphi^{(s)}}(0, z) \right) dz. \quad (\text{S.5.6})$$

Here we deduce from (S.5.6), after lengthy algebra,

$$\begin{aligned} C^{(s,p)} &= -\frac{\ell d \hat{\rho} (1 - \hat{\rho})}{2(L - \ell)^2} + \frac{2\hat{\rho}d^3 \sin^2(kL/2)}{\ell(L - \ell)^2} \left(\frac{\hat{\rho}^3}{4} - \frac{\hat{\rho}^2}{3} + (1 - \hat{\rho}) \left(\frac{\hat{\rho}}{Kd} + \frac{\ell^2}{6d^2} \right) \right) \\ &+ \frac{4}{d\ell(L - \ell)^2} \sum_{m=1}^{\infty} \frac{(1 - (-1)^m \cos kL)(1 - \cosh(\alpha_m \hat{\rho}d) + (\frac{1}{2} - \hat{\rho})\alpha_m d \sinh(\alpha_m \hat{\rho}d))}{\alpha_m^4 ((\alpha_m/K) \sinh(\alpha_m \hat{\rho}d) - \cosh(\alpha_m \hat{\rho}d))}. \end{aligned} \quad (\text{S.5.7})$$

We remark that a calculation of $C^{(s,p)}$ reveals it to be identical to $C^{(p,s)}$, which is expected by reciprocity.

5.1 Numerical approximation

We have

$$A^{(s,p)} \approx \sum_{n=0}^N A_n^{(s)} \overline{E_n^{(p)}} \quad (\text{S.5.8})$$

and

$$A^{(p,s)} \approx \sum_{n=0}^N A_n^{(p)} \overline{E_n^{(s)}} \quad (\text{S.5.9})$$

and, of course, $A^{(p,s)} = \overline{A^{(s,p)}}$, for reasons already detailed.

5.2 Asymptotic results for small gaps

First we note from (S.5.7) that

$$C^{(p,s)} \approx \frac{1}{\epsilon} \frac{2\hat{\rho}^2 d^2 \sin^2(kL/2)}{L^2} \left(\frac{\hat{\rho}^2}{4} - \frac{\hat{\rho}}{3} + \frac{(1-\hat{\rho})}{Kd} \right) \quad (\text{S.5.10})$$

The leading order approximation to the solution of the integral equation is used to find

$$A^{(p,s)} \approx \frac{1}{\epsilon^3} \frac{\tilde{G}^{(p)} \overline{\tilde{G}^{(s)}}}{\tilde{T}}. \quad (\text{S.5.11})$$

Using (S.1.22), (S.3.31) and (3.35) and simplifying, we can combine our result with (S.5.10) in (S.5.4) to get

$$F^{(s,p)} = \frac{1}{\epsilon} \frac{\hat{\rho}^2 d}{KL^2} \left(2Kd \left(\frac{\hat{\rho}^2}{4} - \frac{\hat{\rho}}{3} + \frac{1-\hat{\rho}}{Kd} \right) - \frac{K\hat{\rho}d-2}{\frac{K\hat{\rho}d-1}{Kd} + \frac{1}{2}\epsilon \cot\left(\frac{kL}{2}\right)} \left(\frac{\hat{\rho}^2}{3} - \frac{\hat{\rho}}{2} + \frac{1-\hat{\rho}}{Kd} \right) \right) \sin^2\left(\frac{kL}{2}\right). \quad (\text{S.5.12})$$

Appendix A: Evaluation of infinite series

In this Appendix we establish three main non-trivial results using the following definitions given in the body of the paper and the supplementary material: $\beta_m = k + 2m\pi/L$,

$$g_m^{(h)} = i(e^{-i\beta_m L} - e^{-i\beta_m \ell})/(\beta_m \ell) \quad (\text{S.A.1})$$

and

$$g_m^{(p)} = \frac{i}{2\beta_m \ell} (e^{-i\beta_m L} + e^{-i\beta_m \ell}) + \frac{1}{\beta_m^2 \ell a} (e^{-i\beta_m L} - e^{-i\beta_m \ell}), \quad (\text{S.A.2})$$

where we have used the abbreviation $a = L - \ell$. Then

$$(i) C^{(h,h)} = \frac{\ell^2}{da} \sum_{m=-\infty}^{\infty} \frac{|g_m^{(h)}|^2}{\beta_m L} = \frac{a \cot(kL/2)}{2d} \quad (\text{S.A.3})$$

is the key result from which it will be shown that

$$(ii) C^{(p,p)} = \sum_{m=-\infty}^{\infty} \frac{|g_m^{(p)}|^2}{\beta_m L} = 0 \quad (\text{S.A.4})$$

and

$$(iii) C^{(p,h)} = \frac{\ell^2}{da} \sum_{m=-\infty}^{\infty} \frac{g_m^{(p)} \overline{g_m^{(h)}}}{\beta_m L} = i \frac{a^2}{12\ell^2}. \quad (\text{S.A.5})$$

First, from (S.A.3) we note that

$$C^{(h,h)} = \frac{L^2}{da} J_1(a), \quad \text{where } J_1(a) = \sum_{m=-\infty}^{\infty} \frac{\sin^2(\beta_m a/2)}{(\beta_m L)^3}. \quad (\text{S.A.6})$$

Then clearly $J(0) = 0$ and

$$J_1'(a) = \frac{2}{L} \sum_{m=-\infty}^{\infty} \frac{\sin(\beta_m a)}{(\beta_m L)^2}, \quad (\text{S.A.7})$$

so that $J_1'(0) = 0$ and then finally

$$J_1''(a) = \frac{2}{L^2} \sum_{m=-\infty}^{\infty} \frac{\cos(\beta_m a)}{\beta_m L}, \quad (\text{S.A.8})$$

which we choose to write as

$$J_1''(a) = \frac{2a}{L^3} \sum_{m=-\infty}^{\infty} \frac{\cos(ka + \lambda m)}{ka + \lambda m}, \quad (\text{S.A.9})$$

where we let $\lambda = 2\pi a/L$ so $0 < \lambda < 2\pi$. Now consider the function

$$F(z) = \frac{\pi \cos(ka + (\lambda - \pi)z)}{(ka + \lambda z) \sin(\pi z)}. \quad (\text{S.A.10})$$

Clearly $F(z)$ has poles at $z = n \in \mathbb{Z}$ and at $z = -ka/\lambda = -kL/2\pi$ where we have assumed $kL \neq 2\pi n$ so all poles are simple poles. If we let $z = Re^{i\theta}$, it is clear that as $|z| \rightarrow \infty$ (i.e. $R \rightarrow \infty$) that we have

$$|F(z)| \sim \frac{\pi e^{|\lambda - \pi||z|}}{\lambda |z| e^{\pi|z|}}, \quad (\text{S.A.11})$$

which is clearly exponentially decaying and thus we can write

$$0 = \lim_{N \rightarrow \infty} \oint_{C_N} F(z) dz \quad (\text{S.A.12})$$

where C_N is a circle of radius $N + \frac{1}{2}$ centred on the origin of the complex plane. Computing the residues inside C_N and letting $N \rightarrow \infty$ results in the identity

$$\sum_{m=-\infty}^{\infty} \frac{\cos(ka + \lambda m)}{ka + \lambda m} = \frac{L}{2a} \cot\left(\frac{kL}{2}\right). \quad (\text{S.A.13})$$

Thus, we have established that

$$J_1''(a) = \frac{1}{L^2} \cot\left(\frac{kL}{2}\right). \quad (\text{S.A.14})$$

Integrating twice with respect to a and applying the conditions $J_1'(0) = J_1(0) = 0$ gives

$$J_1(a) = \frac{a^2}{2L^2} \cot\left(\frac{kL}{2}\right) \quad (\text{S.A.15})$$

and (i) follows.

In order to calculate result (ii) start with the definition

$$J_2(a) = \sum_{m=-\infty}^{\infty} \frac{\cos^2(\beta_m a/2)}{(\beta_m L)^3} \quad (\text{S.A.16})$$

and so we can write

$$J_2(a) = \sum_{m=-\infty}^{\infty} \frac{1}{(\beta_m L)^3} - \sum_{m=-\infty}^{\infty} \frac{\sin^2(\beta_m a/2)}{(\beta_m L)^3} = \frac{1}{8} \cot\left(\frac{kL}{2}\right) \operatorname{cosec}^2\left(\frac{kL}{2}\right) - \frac{1}{4} J_1(a), \quad (\text{S.A.17})$$

using Gradshteyn and Ryzhik (1981). Additionally, let us define

$$J_3(a) = \sum_{m=-\infty}^{\infty} \frac{\sin(\beta_m a/2) \cos(\beta_m a/2)}{(\beta_m L)^4} \quad (\text{S.A.18})$$

so that

$$J_3'(a) = \frac{1}{2L} \sum_{m=-\infty}^{\infty} \frac{1}{(\beta_m L)^3} - \frac{1}{4L} J_1(a) = \frac{1}{16L} \cot\left(\frac{kL}{2}\right) \left(\operatorname{cosec}^2\left(\frac{kL}{2}\right) - \frac{2a^2}{L^2} \right). \quad (\text{S.A.19})$$

Integrating with respect to a and applying $J_3(a) = 0$ gives

$$J_3(a) = \frac{a}{16L} \cot\left(\frac{kL}{2}\right) \left(\operatorname{cosec}^2\left(\frac{kL}{2}\right) - \frac{2}{3} \frac{a^2}{L^2} \right). \quad (\text{S.A.20})$$

Finally, letting

$$J_4(a) = \sum_{m=-\infty}^{\infty} \frac{\sin^2(\beta_m a/2)}{(\beta_m L)^5} \quad (\text{S.A.21})$$

we see that $J_4'(a) = J_3(a)/L$ and $J_4(a) = 0$ so that we can deduce

$$J_4(a) = \frac{a^2}{32L} \cot\left(\frac{kL}{2}\right) \left(\operatorname{cosec}^2\left(\frac{kL}{2}\right) - \frac{1}{3} \frac{a^2}{L^2} \right). \quad (\text{S.A.22})$$

From the definition (S.A.4) we find that

$$C^{(p,p)} = \sum_{m=-\infty}^{\infty} \frac{|g_m^{(p)}|^2}{\beta_m L} = \frac{aL^2}{\ell^2} J_2(a) - \frac{4L^3}{\ell^2} J_3(a) + \frac{4L^4}{\ell^2 a} J_4(a) \quad (\text{S.A.23})$$

and (iii) follows.

Moving on, we define

$$J_5(a) = \sum_{m=-\infty}^{\infty} \frac{\cos(\beta_m a)}{(\beta_m L)^4} \quad (\text{S.A.24})$$

so that $J_5(0) = 0$ and

$$J_5'(a) = \frac{1}{L} \sum_{m=-\infty}^{\infty} \frac{\cos(\beta_m a)}{(\beta_m L)^2} \quad (\text{S.A.25})$$

so that $J_5'(0) = (1/4L)\operatorname{cosec}^2(kL/2)$. Finally,

$$J_5''(a) = \frac{1}{L^2} \sum_{m=-\infty}^{\infty} \frac{\sin(\beta_m a)}{\beta_m L} \quad (\text{S.A.26})$$

or

$$J_5''(a) = -\frac{a}{L^3} \sum_{m=-\infty}^{\infty} \frac{\sin(ka + \lambda m)}{ka + \lambda m} \quad (\text{S.A.27})$$

where we have let $\lambda = 2\pi a/L$ so $0 < \lambda < 2\pi$. Similarly to before we define

$$G(z) = \frac{\pi \sin(ka + (\lambda - \pi)z)}{(ka + \lambda z) \sin(\pi z)} \quad (\text{S.A.28})$$

so that $G(z)$ has poles at $z = n \in \mathbb{Z}$ and at $z = -ka/\lambda = -kL/2\pi$ and we assume $kL \neq 2\pi n$ so all poles are simple poles. Again, it can be shown that $|G(z)| \rightarrow 0$ as $|z| \rightarrow \infty$ and so

$$0 = \lim_{N \rightarrow \infty} \oint_{C_N} G(z) dz \quad (\text{S.A.29})$$

where C_N is a circle of radius $N + \frac{1}{2}$. Calculating the residues from the poles inside C_N and letting $N \rightarrow \infty$ results in

$$\sum_{m=-\infty}^{\infty} \frac{\sin(ka + \lambda m)}{ka + \lambda m} = \frac{\pi}{\lambda} = \frac{L}{2a}. \quad (\text{S.A.30})$$

and hence

$$J_5''(a) = -\frac{1}{2L^2}. \quad (\text{S.A.31})$$

Integrating twice with respect to a and applying our the initial conditions gives

$$J_5(a) = -\frac{a}{4L} \left(\frac{a}{L} + \operatorname{cosec}^2\left(\frac{kL}{2}\right) \right). \quad (\text{S.A.32})$$

Finally consider

$$J_6(a) = \sum_{m=-\infty}^{\infty} \frac{\sin(\beta_m a)}{(\beta_m L)^3} \quad (\text{S.A.33})$$

from which it follows that

$$J_6'(a) = -\frac{1}{L} \sum_{m=-\infty}^{\infty} \frac{\sin(\beta_m a)}{\beta_m L} = -\frac{1}{L} R(a) = \frac{a}{4L^2} \left(\frac{a}{L} + \operatorname{cosec}^2\left(\frac{kL}{2}\right) \right) \quad (\text{S.A.34})$$

and so

$$J_6(a) = \frac{a^2}{24L^2} \left(\frac{2a}{L} + 3 \operatorname{cosec}^2\left(\frac{kL}{2}\right) \right) + J_6(0), \quad (\text{S.A.35})$$

$$C^{(h,p)} = \frac{iL^2}{da} \left(P_5(a) + 2\frac{L}{a} (P_6(a) - P_6(0)) \right). \quad (\text{S.A.36})$$

and the result in (iii) follows.

Appendix B: Another infinite series

We start with

$$\sum_{m=-\infty}^{\infty} \frac{e^{i\beta_m(x-x')}}{\beta_m L} = \sum_{m=-\infty}^{\infty} \frac{\cos(kX + \hat{\lambda}m)}{kX + \hat{\lambda}m} + i \sum_{m=-\infty}^{\infty} \frac{\sin(kX + \hat{\lambda}m)}{kX + \hat{\lambda}m}, \quad (\text{S.B.1})$$

where we have let $X = (x - x') > 0$ (without loss of generality) and $\hat{\lambda} = 2\pi X/L$ such that $0 < X \leq \ell$ and $0 < \hat{\lambda} < 2\pi$. Using (S.A.13) and (S.A.30) from Appendix A we have

$$\sum_{m=-\infty}^{\infty} \frac{e^{i\beta_m X}}{\beta_m L} = \frac{1}{2} \left(\cot\left(\frac{kL}{2}\right) + i \right). \quad (\text{S.B.2})$$

Conjugating this result is the same as reversing the sign of X and if $X = 0$ the series is real. Then the general result is

$$\sum_{m=-\infty}^{\infty} \frac{e^{i\beta_m(x-x')}}{\beta_m L} = \frac{1}{2} \cot\left(\frac{kL}{2}\right) + \frac{i}{2} \text{sgn}(x - x'). \quad (\text{S.B.3})$$

where $\text{sgn}(X) = -1, 0, 1$ when $X < 0, X = 0, X > 0$ respectively.